Přílohy

Tabulky odprašování zrn

T1. Odprašování SiO_2 zrna pomocí 2 keV Ar iontů při nízkém povrchovém potenciálu drženém 1 keV elektrony. Sloupeček označený Faraday uvádí celkový signál z Faradayova válce, sloupeček Proud uvádí parametr B z rovnice 5.1, zde uvedené výtěžky jsou počítány pro každé odprašování, ale vzhledem k přesnosti určení hmotnosti (m_{err}) je výsledný odprašovací výtěžek získán lineární regresí ze závislosti hmoty zrna na počtu dopadlých iontů.

T2. Odprašování SiO_2 zrna pomocí 3 keV Ar iontů při vysokém povrchovém potenciálu. Počet dopadlých iontů byl vypočítán pomocí korekce dle rovnice 5.2.

T3. Odprašování SiO_2 zrna pomocí 3 keV Ar iontů při střední (≈41 C/kg), vysokém (≈69 C/kg) a nízkém (≈0,4 C/kg) povrchovém potenciálu.

T4. Naměřená data při pokusu o odprašování SiO_2 zrna pomocí 2 keV He iontů při nízkém povrchovém potenciálu drženém 1 keV elektrony.

Zrno	T [h]	T_{celk} [h]	Faraday [V·s]	Proud [C/V·s·kg]	Ionty [10^8]	$Ionty_{celk}$ [10^8]	m [10^{-15} kg]	m_{err} [10^{-17} kg]	m [10^{-15} kg]	Výtěžek [amu/ion]	Výtěžek [SiO_2/ion]
140121	0		0	0	0	0	1.190	6.7	—	—	—
	1.15	1.15	13501	0.926	0.928	0.928	1.176	2.2	1.4	91	1.51
	3.47	4.62	41363	0.838	2.545	3.473	1.135	1.8	4.1	97	1.61
	4.59	9.21	55972	0.970	3.845	7.318	1.079	4.0	5.6	88	1.46
	4.64	13.86	58051	0.935	3.656	10.975	1.022	2.8	5.7	94	1.56
	2.89	16.74	35209	0.965	2.168	13.142	0.988	1.4	3.4	94	1.56
	4.78	21.53	58059	0.979	3.506	16.648	0.938	4.0	5.0	87	1.44
	4.22	25.74	52063	1.001	3.050	19.698	0.893	0.6	4.5	88	1.47
	2.58	28.33	30955	0.997	1.721	21.419	0.868	0.2	2.6	89	1.48
	2.68	31.00	31167	1.009	1.704	23.123	0.845	1.5	2.3	81	1.34
	5.69	36.69	70184	0.991	3.658	26.781	0.787	0.9	5.8	96	1.60
	3.26	39.95	39662	1.235	2.406	29.187	0.757	1.4	3.0	74	1.24
	3.51	43.46	42053	1.041	2.068	31.255	0.731	0.2	2.6	76	1.27
	3.75	47.21	44199	1.058	2.133	33.388	0.693	1.9	3.8	106	1.77
	2.60	49.81	30965	0.995	1.332	34.720	0.672	3.3	2.1	95	1.59
	4.08	53.89	46047	1.008	1.948	36.668	0.638	1.7	3.4	105	1.75
	4.23	58.12	48695	1.070	2.075	38.743	0.607	2.2	3.1	89	1.48
	3.19	61.31	33424	1.233	1.562	40.305	0.584	1.9	2.4	92	1.53
	4.07	65.38	41780	1.006	1.530	41.835	0.558	1.3	2.5	100	1.66
	4.27	69.65	44143	1.345	2.069	43.904	0.532	1.7	2.6	77	1.28
	4.27	73.91	49019	1.144	1.861	45.765	0.504	1.5	2.8	91	1.52
	4.23	78.15	45311	1.283	1.828	47.593	0.479	2.3	2.4	80	1.34
	4.92	83.07	56829	1.159	1.971	49.563	0.448	1.1	3.2	97	1.61
	5.14	88.20	55215	1.298	2.003	51.566	0.420	1.7	2.8	83	1.39
	4.52	92.73	47492	1.201	1.495	53.061	0.397	0.0	2.3	94	1.57
	4.23	96.96	44364	1.178	1.294	54.354	0.376	0.8	2.1	95	1.59
	4.17	101.13	44308	1.210	1.259	55.613	0.356	0.8	2.0	94	1.57

T1. Odprašování SiO_2 zrna pomocí 2 keV Ar iontů při nízkém povrchovém potenciálu drženém 1 keV elektrony. Sloupeček označený Faraday uvádí celkový signál z Faradayova válce, sloupeček Proud uvádí parametr B z rovnice 5.1, zde uvedené výtěžky jsou počítány pro každé odprašování, ale vzhledem k přesnosti určení hmotnosti (m_{err}) je výsledný odprašovací výtěžek získán lineární regresí ze závislosti hmoty zrna na počtu dopadlých iontů.

Zrno	T [h]	T_{celk} [h]	Q/m [C/kg]	Korekce	Faraday [V·s]	Proud [C/V·s·kg]	Ionty [10^8]	$Ionty_{celk}$ [10^8]	m [10^{-15} kg]	m_{err} [10^{-17} kg]	m [10^{-15} kg]	Výtěžek [amu/ion]	Výtěžek [SiO_2/ion]
140823	0.00	0.00	0.0		0	0	0	0	1.405	2.9	—	—	—
	2.49	2.49	38.5	0.73	18493	0.591	0.701	0.701	1.386	2.3	1.9	163	2.72
	4.25	6.74	55.3	0.62	36241	1.242	2.400	3.101	1.361	3.4	2.5	63	1.04
	4.90	11.64	59.1	0.59	42266	1.233	2.609	5.710	1.333	4.3	2.8	65	1.08
	4.39	16.03	62.7	0.56	34609	1.256	2.043	7.753	1.317	1.2	1.6	47	0.79
	5.27	21.30	61.2	0.58	40479	1.295	2.479	10.232	1.294	2.7	2.3	56	0.93
	4.86	26.16	61.4	0.57	36674	1.242	2.111	12.344	1.269	1.3	2.5	71	1.19
	5.07	31.23	64.0	0.56	39031	1.262	2.168	14.512	1.245	2.5	2.4	67	1.11
	6.27	37.50	60.0	0.58	49034	1.366	3.037	17.549	1.226	0.8	1.9	38	0.63
	5.11	42.61	64.3	0.55	38534	1.349	2.201	19.750	1.192	1.1	3.4	93	1.55
	5.14	47.75	62.7	0.56	39006	1.311	2.148	21.898	1.180	4.9	1.2	34	0.56

T2. Odprašování SiO_2 zrna pomocí 3 keV Ar iontů při vysokém povrchovém potenciálu. Počet dopadlých iontů byl vypočítán pomocí korekce dle rovnice 5.2. Vysvětlení ostatních sloupečků je u tabulky T1.

Zrno	T [h]	T_{celk} [h]	Q/m [C/kg]	Korekce	Faraday [V·s]	Proud [C/V·s·kg]	Ionty [10^8]	$Ionty_{celk}$ [10^8]	m [10^{-15} kg]	m_{err} [10^{-17} kg]	m [10^{-15} kg]	Výtěžek [amu/ion]	Výtěžek [SiO_2/ion]
141001	0	0	0		0	0	0	0	1.358	3.4	—	—	—
	1.76	1.76	59.2	0.59	14412	1.442	1.037	1.037	1.327	3.6	3.1	180	3.00
	5.19	6.95	40.9	0.72	45534	1.395	3.767	4.804	1.275	1.9	5.2	83	1.38
	5.22	12.18	41.3	0.71	45295	1.393	3.583	8.387	1.231	4.9	4.4	74	1.23
	5.13	17.31	42.5	0.70	41908	1.358	3.081	11.468	1.176	0.6	5.5	108	1.79
	5.19	22.50	40.9	0.72	40825	1.386	2.975	14.443	1.151	1.1	2.5	51	0.84
	5.12	27.62	67.0	0.53	34910	1.526	2.046	16.489	1.138	3.6	1.3	38	0.64
	5.13	32.75	71.3	0.51	34727	1.446	1.802	18.290	1.125	1.5	1.3	43	0.72
	5.08	37.83	68.5	0.52	34683	1.426	1.821	20.111	1.099	1.6	2.6	86	1.43
	4.92	42.75	67.2	0.53	33996	1.606	1.999	22.110	1.074	1.3	2.5	75	1.25
	5.15	47.90	0.4	1.00	22133	1.385	2.055	24.165	1.040	2.7	3.4	100	1.66

T3. Odprašování SiO_2 zrna pomocí 3 keV Ar iontů při středním (≈41 C/kg), vysokém (≈69 C/kg) a nízkém (≈0,4 C/kg) povrchovém potenciálu.

Zrno	T [h]	T_{celk} [h]	Faraday [V·s]	Proud [C/V·s·kg]	Ionty [10^8]	$Ionty_{celk}$ [10^8]	m [10^{-15} kg]	m_{err} [10^{-17} kg]	m [10^{-15} kg]	Výtěžek [amu/ion]	Výtěžek [SiO_2/ion]
140320	0	0	0	0	0	0	1.350	2.5	—	—	—
	1.56	1.56	16824	1.440	2.042	2.042	1.346	5.1	0.4	12	0.20
140324	0	0	0	0	0	0	1.287	4.9	—	—	—
	2.16	2.16	21029	1.533	2.590	2.590	1.282	3.8	0.5	12	0.19
	5.08	7.24	31190	1.188	2.966	5.556	1.281	4.4	0.1	2	0.03
	2.34	9.58	18114	1.450	2.101	7.657	1.282	2.2	-0.1	-3	-0.05
	3.20	12.78	24364	1.315	2.564	10.221	1.275	3.0	0.7	16	0.27
	3.92	16.70	59413	1.193	5.641	15.861	1.264	3.9	1.1	12	0.20
140328	0	0	0	0	0	0	1.291	2.6	—	—	—
	0.62	0.62	9068	1.235	0.903	0.903	1.286	0.6	0.5	33	0.56
	3.46	4.09	21348	1.453	2.490	3.392	1.277	5.5	0.9	22	0.36

T4. Naměřená data při pokusu o odprašování SiO_2 zrna pomocí 2 keV He iontů při nízkém povrchovém potenciálu drženém 1 keV elektrony.

Přiložené publikace

A1 [8]
Beránek, M., Vyšinka, M., Pavlů, J., Richterová, I., Němeček, Z., a Šafránková, J., Dust as a Gas Carrier. *IEEE Trans. Plasma Sci.*, 2010, **38**(4), 886–891. DOI 10.1109/TPS.2009.2038219

A2 [101]
Vyšinka, M., Vaverka, J., Pavlů, J., Němeček, Z., a Šafránková, J., Depth Profiles of Ions Implanted into Spherical Dust Grains—a TRIM Based Model. In: Safrankova, J. a Pavlu, J. (Eds.) *WDS'09 Proceedings of Contributed Papers: Part II - Physics of Plasmas and Ionized Media*, Prague, Matfyzpress, 2009, pp. 195–201. ISBN 978-80-7378-102-6.

A3 [99]
Vyšinka, M., Němeček, Z., Šafránková, J., Pavlů, J., Vaverka, J., a Lavková, J., Sputtering of Spherical SiO_2 Samples. *IEEE Trans. Plasma Sci.*, 2016, **44**(6), 1036–1044. DOI 10.1109/TPS.2016.2564502

A4 [118]
Vyšinka, M., Nouzák, L., Pavlů, J., Němeček, Z., Šafránková, J., a Richterová, I. MF Microspheres: Helping or Puzzling Tool? *IEEE Trans. Plasma Sci.*, 2017, odesláno do tisku

Příloha A1.

Beránek, *M.,* Vyšinka, *M.,* Pavlů, *J.,* Richterová, *I.,* Němeček, *Z., a* Šafránková, *J., Dust as a Gas Carrier.* IEEE Trans. Plasma Sci., *2010,* **38***(4), 886–891. DOI 10.1109/TPS.2009.2038219*

Dust as a Gas Carrier

Martin Beránek, Marek Vyšinka, Jiří Pavlů, Ivana Richterová, Zdeněk Němeček, and Jana Šafránková

***Abstract*—Dust in space can collect particles from surrounding plasma and transport them over long distances. Release of the implanted particles can then change the mass composition in a particular place of the space. The depth of ion penetration into the dust body strongly depends on an initial mutual energy and differs with ion species as well as with the grain composition. The same holds for diffusion constant of implanted ions (already neutralized) exiting back to the free space. We have used our measurements of the release of Ar ions implanted into glassy carbon dust grains for determination of the diffusion coefficient. Our calculations provide the limits for the amount of gas that can be dissolved in the grain as well as its release rate. We discuss the influence of the dust sputtering and dust temperature on the aforementioned quantities.**

***Index Terms*—Dust charging, gas diffusion, interplanetary dust.**

I. Introduction

DUST as a common constituent of space as well as laboratory plasmas is bombarded by energetic ions (e.g., dust in the solar wind is exposed to H^+ of about 1 keV, He^{++} of about 4 keV, etc.). Ions not only modify and sputter the dust surface but also can penetrate into the material of the grain itself. Then, the diffusion starts to release atoms, and its rate depends on the diffusion coefficient that is generally an exponential function of temperature.

In the interplanetary space, the dissolved ions (already neutralized) could be transported in the dust safely across long distances due to a low temperature. Once the gas leaves the grain, it becomes usually ionized again quickly by solar UV or by charge exchange. The ions are picked up by the interplanetary magnetic field and carried outward with the solar wind as a distinct component of the solar wind called pick-up ions [1]. Pick-up ions are often considered to be produced by ionization of neutral interstellar gas that penetrates the solar system [2]. Dust interactions with the solar wind provide a further source that contributes to a different elemental composition of the pick-up ion population. Pick-up ions are clearly identifiable due to their distinctive charge state and velocity distribution [3]. Dust may contribute to the formation of pick-up ions through a number of processes: 1) sublimation of the grain material; 2) sputtering of the grain due to an ion bombardment; 3) by recycling of solar-wind particles into pick-up ions by adsorption and desorption; and 4) by release of the atoms that were previously implanted and stored in the grain.

It is known that the surface layers of lunar samples are doped with solar-wind particles. Banks [4] studied theoretically this effect for dust grains. Rajan *et al.* [5] reported large ^{4}He concentrations in collected micrometeorites (e.g., small interplanetary particles which enter the Earth's atmosphere without being melted by frictional heating), and the authors concluded that this helium comes from the implanted solar wind. Nier [6] performed experiments to determine the amount and isotopic composition of helium and neon found in individual interplanetary dust particles collected in the Earth's stratosphere in order to distinguish between particles of cometary and asteroidal origin. He found that the ^{4}He degassing pattern of the dust is comparable to that of the lunar samples. However, while implantation of heavier ions would also be expected, heavier elements have not been measured. Based on observations of solar-wind implantation, Fahr *et al.* [7] suggested that the implantation of solar-wind particles into the surface layer of dust can lead to subsequent desorption of neutrals. They predicted that, inside 0.5 AU (0.05 AU, respectively), the density of neutral hydrogen (helium, respectively) produced by this process exceeds that of the interstellar hydrogen (helium, respectively) found at these distances from the Sun. The amount of dust-generated neutral molecular hydrogen was calculated by Gruntman [8]. He considered the efficiency of various processes for conversion of the H_2 molecules to H_2^+ ions and their subsequent destruction. He concluded that a significant part of H_2^+ ions should survive and make unique molecular pick-up ions.

Vernazza *et al.* [9] analyzed the sources of reddening of asteroid surfaces. They concluded that implantation of solar-wind ions is the favorite mechanism causing reddening. Plainaki *et al.* [10] modeled space weathering processes that take place on the surfaces of near-Earth objects. Starukhina [11] studied deposition of solar-wind ions on the surface of Moon. She identified polar regions as possible repositories of gases related to the solar wind.

In the laboratory plasma, e.g., in tokamaks, dust can accommodate plasma ions—retention of tritium and deuterium being particularly important for safety reasons [12]. Yoshida *et al.* [13] studied the carbon–tungsten dust prepared by deuterium arc discharge and measured the desorption rate of heated samples. They concluded that the deuterium concentration in the carbon dust was estimated to be 0.2 of the atomic ratio (D/C) and even higher in carbon–tungsten grains, and they suggested to increase the temperature of the outer walls. Since the dust is charged, it moves and accelerates within the tokamak [14]. Rudakov *et al.* [15] examined a migration of dust in the DIII-D tokamak, and they gave an experimental evidence that a

Manuscript received July 10, 2009; revised October 29, 2009. First published January 19, 2010; current version published April 9, 2010. This work was supported in part by the Research plan MSM 0021620860 financed by the Ministry of Education of the Czech Republic, by the Czech Grant Agency under Contracts 202/08/P066 and 202/08/H057, and by the Grant Agency of Charles University (GAUK 146207).

The authors are with the Department of Surface and Plasma Science, Faculty of Mathematics and Physics, Charles University, 180 00 Prague, Czech Republic (e-mail: jiri.pavlu@mff.cuni.cz).

Digital Object Identifier 10.1109/TPS.2009.2038219

micrometer-sized carbon dust contained in a tokamak divertor can become highly mobile and reach the core plasma. However, a dust contribution to the core contamination is still unclear.

As a side effect of measurements of sputtering yields, it was also found recently [16] that carbon traps ions at the surface more efficiently than metallic materials, which may significantly bias mass loss measurements on samples that have been subjected to high irradiation doses (Xe^+ in this particular case).

Based on these observations, we can expect that the mass of the dust grain exposed to the ion bombardment can increase with time as the sputtering could be less efficient than trapping in some cases. These ions (now neutrals) can later diffuse within the grain and leave it when they reach the surface. In this paper, we focus on the observation of the diffusion and successive desorption of Ar ions in the micrometer-sized amorphous carbon sphere. The mass-change rate is evaluated and successfully modeled.

II. Experiment

The experiment has been performed on a single glassy carbon grain trapped inside the cylindrical quadrupole electrodynamic trap. The frequency of the grain oscillations inside the trap is proportional to the ratio of the grain charge and its mass [17], [18]. Special techniques described in [19] can be used for determination of the other parameters of the investigated grain. The optical detection of the motion of the grain and electrical damping of its oscillations allow us to perform measurement under UHV conditions $(10^{-7}$ Pa) and hold the grain in the trap for a long period (on the order of weeks) [17]–[19].

The analyzed spherical glassy carbon samples have been produced by HTW Hochtemperatur-Werkstoffe. The diameter of the grains lies between 1 and 5 μm. According to the specification of the manufacturer, grains are amorphous and isotropic with the mass density of 1500 kg/m^3. The specific resistance $(50\ \Omega \cdot \mu\text{m})$ is low enough to prevent the presence of electric field inside the grain.

The glassy carbon grain with a mass of $(6.27 \pm 0.01) \cdot 10^{-15}$ kg and a diameter of 1.93 μm has been trapped and treated with an Ar^+ beam for 8 h. The energy of impinging ions was 7 keV. The total current of ions has been approximately 35 000 particles per second, and the corresponding beam intensity is on the order of nanoamperes per square millimeter. This value was determined from the initial field ion emission current measured on another grain after switching the ion gun off.

The surface potential of the grain was held low enough to eliminate the ion field emission [20] using simultaneous electron bombardment. After the treatment, the grain was held in the trap for a few days, and its charge-to-mass ratio was continuously monitored. According to our previous observations [19], the charge of the trapped grain remains constant over days when there is neither field emission nor beams of charged particles. Because of the constant charge of the grain, we attributed the observed changes of specific charge to variations of the grain mass. Note that we can observe relative changes of the mass on the order of 10^{-4}. This long-term stability has been achieved subtracting the temperature drift.

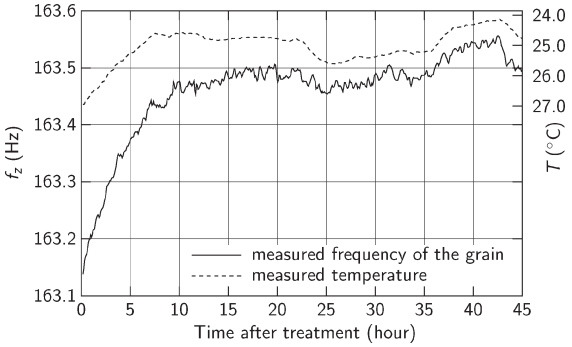

Fig. 1. Measured frequency of oscillations of the grain and the ambient temperature.

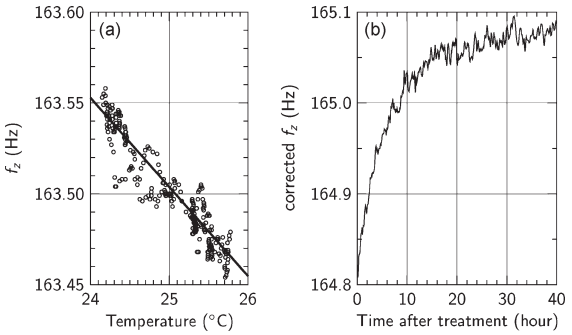

Fig. 2. (a) Correlation between the temperature and frequency after 25th hour. (b) Frequency of the grain corrected for the temperature drift.

A. Correction of the Temperature Drift

In our experiment, there are many devices and circuits that are potentially sensitive to the change of temperature. It is not possible to analyze each device independently; therefore, we found out an appropriate temperature correction experimentally through the following procedure: We have measured the frequency of the grain oscillation together with the ambient temperature (Fig. 1). Under the assumption that there is no measurable change in the charge-to-mass ratio after a sufficiently long time, we fit a linear dependence between the measured temperature and oscillation frequency starting at 25th hour after treatment [Fig. 2(a)], when the frequency copies the measured temperature (compare the lines in Fig. 1). Furthermore, we have applied this fit to correct the measured frequency in the full range of time [Fig. 2(b)]. We suggest that the remaining roughly exponential increase of the frequency (which is directly proportional to the charge-to-mass ratio) after the treatment is caused by deposited Ar atoms leaving the grain due to diffusion.

III. Diffusion Coefficient

We have utilized a simple model of diffusion to find a diffusion coefficient D. We neglect the surface effects and compute the diffusion inside the homogeneous grain. Since the

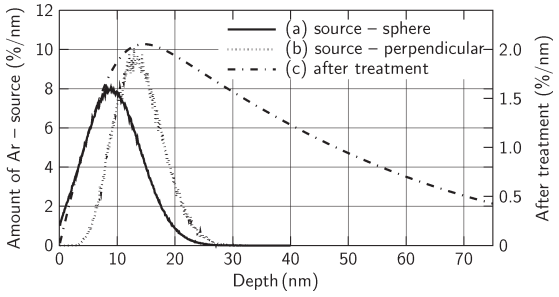

Fig. 3. [(a) and (b)] Probability of deposition of the 7-keV Ar ion in a given depth (left axis) and computed by the SRIM code [21]. (c) Distribution of Ar after 8 h of treatment (right axis). $D = 5 \cdot 10^{-16}$ cm^2/s and $N = 35\,000$ s^{-1}.

problem has a radial symmetry, the general equations of the diffusion can be written as

$$\frac{\partial \rho}{\partial t} = D \frac{1}{r} \cdot \frac{\partial^2}{\partial r^2}(r\rho) \tag{1}$$

$$J = -D \frac{\partial \rho}{\partial r} \tag{2}$$

where ρ is the mass density and J is the mass flux. The density of gas outside the spherical grain is set to zero in our model; therefore, the mass of argon leaving the grain of radius R due to the diffusion according to (2) is

$$\frac{dm}{dt} = 4\pi R^2 \cdot D \cdot \left.\frac{\partial \rho}{\partial r}\right|_{r=R}. \tag{3}$$

During the treatment, there is an additional source term representing the incoming argon ions. We have computed the distribution $f(x)\,dx$ of the impinging ions deposited in a given depth under the surface by the SRIM code [21], [22]. We suppose that the grain rotation in the trap is fast enough to distribute the incoming ions with a radial symmetry. The radial distribution of 7-keV Ar ions is shown in Fig. 3. The dotted line stands for the profile provided by the SRIM code that expects a perpendicular impact of ions. The full line considers the effect of varying incident angles over the sphere [23].

Having the total number of impinging ions per second, i.e., N, we can modify (1) in the following way:

$$\frac{\partial \rho}{\partial t} = D \frac{1}{r} \cdot \frac{\partial^2}{\partial r^2}(r\rho) + \frac{N m_{\mathrm{Ar}} f(R-r)}{4\pi r^2} \tag{4}$$

where R is radius of the grain and $m_{\mathrm{Ar}} = 6.64 \cdot 10^{-26}$ kg is the mass of the argon atom. $f(R-r)$ represents a source term shown in Fig. 3 (profile a). The analytic expression of the source term is unknown; nevertheless, we can solve the equations numerically.

We have modeled the conditions in our experiments, i.e., the 8-h-long treatment (4) and the subsequent diffusion without the source term (1). Distribution of argon just after the treatment is shown in Fig. 3 as the dashed-dotted line.

The results of our model for various values of diffusion coefficients have been compared to the measured data. We are not able to measure the change of mass during the treatment, but

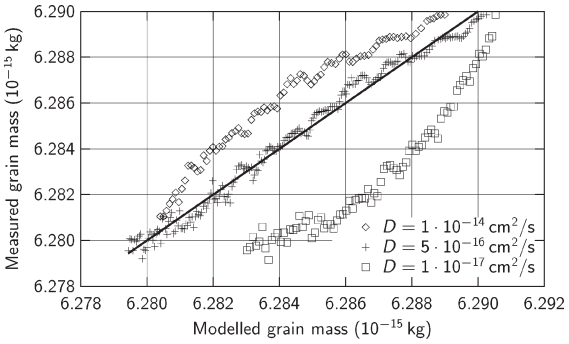

Fig. 4. Relation between the measured mass of the grain and the modeled mass at the same time after treatment for three diffusion coefficients.

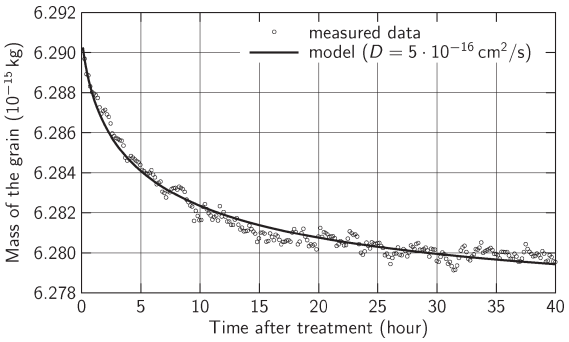

Fig. 5. Change of the grain mass in time. The parameters of the model ($D = 5 \cdot 10^{-16}$ cm^2/s, treatment: 8 h, incident current: 32 400 particles per second) are chosen according to the best fit in Fig. 4.

we compare the model and measured data in the period after the treatment. A modeled mass of the grain versus measured mass at the same time is shown in Fig. 4 for three values of D. The uncertainty of absolute values of the primary current and the final mass of the grain imply uncertainty of the linear scaling of the model result. Nevertheless, the relation is close to linear for the diffusion coefficient, $D = 5 \cdot 10^{-16}$ cm^2/s only, and the value of incident current, 32 400 particles per second, is in good agreement with the value estimated from other measurements. The value of diffusion coefficient will be used in further considerations. In order to demonstrate the agreement between measurement and model, the data from Fig. 4 are replotted in Fig. 5 that compares the computed and measured temporal changes of the grain mass.

IV. Amount of the Gas Dissolved

A. Stable Solution of Diffusion Equation

In our experiment, we have implanted more than 10^{-17} kg of argon into a single 2-μm glassy carbon grain. This is approximately 0.2% of the total mass. The majority of the gas is dissolved in a thin layer at the surface (see Fig. 3, curve c). The mass fraction of Ar in this layer was about 1%.

After a long treatment, the equilibrium state would be reached when the amount of gas inside the grain remains

constant over time. The diffusion equation without a source term (1) is valid for $(R-r)$ that is higher than the implantation depth, i.e., approximately 50 nm. This equation can be solved analytically. Angularly independent solution without singularity at the origin is a constant density. The particular value of this density depends on the boundary conditions which are set by the source term in the thin surface layer. The equilibrium density of gas inside the grain is constant in the majority of grain and decreases in the thin layer at the surface (note that, in equilibrium state, there cannot be any flux toward the center). The actual density and its decrease at the surface have been obtained numerically.

We numerically found the stable solution of (4)

$$\frac{d^2}{dr^2}\left(r\rho(r)\right) = -\frac{N m_{\mathrm{Ar}}}{D}\cdot\frac{f(R-r)}{4\pi r^2} \tag{5}$$

in the range of the implantation depth. The conservation of total mass of the gas inside the grain gives us the second boundary condition at the surface

$$\left.\frac{d\rho(r)}{dr}\right|_R = -\frac{N m_{\mathrm{Ar}}}{D}\frac{\int_0^R f(R-r)dr}{4\pi R^2}. \tag{6}$$

The solution of (5) and (6) depends on a spatial distribution of implanted ions and on the grain radius. The primary current and diffusion coefficient act as the multiplicative factor (N/D). The maximum total mass of argon dissolved $m_{\max}$ depends on the diameter of the grain approximately linearly in the case of fixed number of ions hitting the grain, N; in other words, the implanted mass is proportional to the volume of the grain in the case of the fixed ion flux I

$$m_{\max} = \alpha\cdot m_{\mathrm{Ar}}\cdot R\cdot\frac{N}{D} = \alpha\cdot m_{\mathrm{Ar}}\cdot\pi R^3\cdot\frac{I}{D} \tag{7}$$

where R is the radius of the grain, N is the total number of impinging ions per second, D is the diffusion coefficient, and I is the flux of ions (particles per square meter per second). A coefficient α depends on the spatial distribution of implanted ions. An actual value for 7-keV Ar ions on glassy carbon sphere is $\alpha = 3.08\cdot 10^{-7}$ cm. Note that (7) is not an analytical solution of (5) and (6) but the linear fit of the numerical results. The difference between numerically computed mass and fit (7) is approximately 0.5% at $R = 1$ μm and decreases for larger grains where the implantation depth becomes negligible compared to the grain radius.

When we put the parameters of the investigated 2-μm grain into (7), we get

$$m_{\max} = (1.97\cdot 10^{-36}\ \mathrm{kg\cdot cm^2})\cdot N/D = 1.38\cdot 10^{-16}\ \mathrm{kg}. \tag{8}$$

B. Effect of the Sputtering

The grain sputtering and ion implantation act simultaneously, and rates of both processes are directly proportional to the number of impinging ions. However, the sputtering decreases the grain radius and, according to (7), limits the amount of gas that can be dissolved in the grain. The analysis has shown that

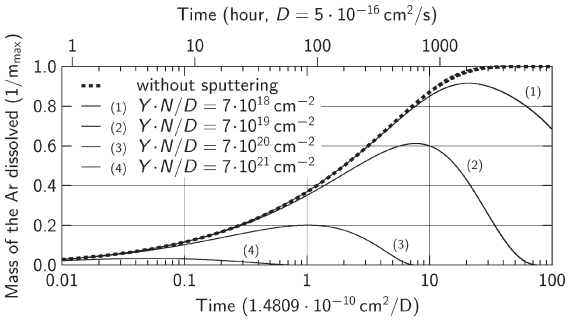

Fig. 6. Modeled increase of the mass of the 2-μm grain under the Ar^+ bombardment due to the dissolved gas and the sputtering of the material of the grain. The vertical axis is scaled with respect to the maximum amount of the gas (7); the scale of the horizontal axis is such that the unit value represents $1/e$ of total mass. The investigated grain is represented by the curve (2). Time in hours is shown for the conditions of our measurement.

the dependences of the mass of the dissolved gas on the time of the grain bombardment can be parameterized by a factor $Y\cdot N/D$, where Y stands for the sputtering yield. The results obtained for several values of $Y\cdot N/D$ are shown in Fig. 6. The dissolved mass is given as a fraction of $m_{\max}$, and the time is scaled by D; thus, the dashed line can be considered as a universal curve describing a temporal evolution of the implanted mass if the sputtering is neglected. The effect of the grain sputtering is demonstrated by profiles computed for different values of $Y\cdot N/D$.

Other parameters influencing the temporal evolution of the dissolved amount of the gas are the grain diameter. Since the dependence on the grain diameter is rather complicated and the computation is time consuming, Fig. 6 shows the results for the 2-μm grain. It allowed us to use other parameters from our experiment ($N = 35\,000\ \mathrm{s^{-1}}$ and $D = 5\cdot 10^{-16}\ \mathrm{cm^2/s}$) and to put the absolute time scale to the top of the panel. Since the sputtering yield for Ar^+ is about unity in the kiloelectronvolt range of energies [24], the line 2 describes the cumulated effect of sputtering, implantation, and diffusion under our experimental conditions.

V. Discussion

The presented numerical results use the value of the diffusion coefficient determined from the experiment. In order to relate this experiment to conditions in the space, we should estimate the dust grain temperature that cannot be directly measured. The temperature of the grain in the vacuum is determined by the radiation balance since the contribution of ion impact to the heating is several orders of magnitude lower. The grain is heated by background environment radiation ($T_{\mathrm{bg}} \approx 300$ K) and by the laser beam (635 nm, with an approximate beam intensity of 1.7 mW/mm^2). The incoming power is compensated by the grain thermal radiation.

We have utilized the MiePlot software [25], [26] to compute the spectral emissivity of the grain. The refractive index of the glassy carbon was set according to [27] and [28]. We integrated the product of emissivity and spectral intensity of a black body radiation over the range of wavelengths, and we

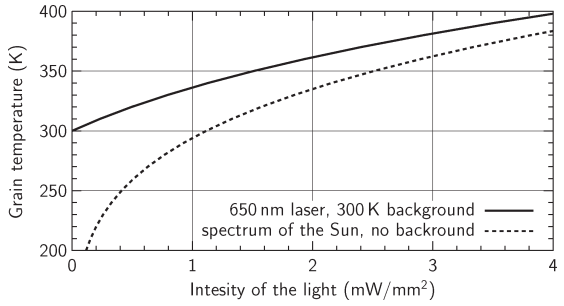

Fig. 7. Equilibrium temperature of glassy carbon grain (2 μm in diameter) illuminated (solid line) by the monochromatic 635-nm light and (dashed line) by the Sun light.

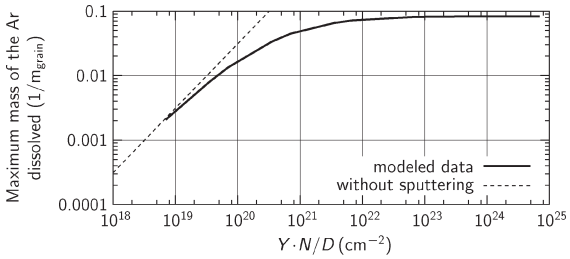

Fig. 8. Maximum amount of Ar dissolved in the 2-μm grain related to the original mass of the grain m_{grain}. Both diffusion and sputtering have been taken into account.

scaled the result to the grain surface area. The result is the total radiated power at a given temperature. A power of the laser beam is multiplied by the emissivity factor ($\varepsilon_{635\ \mathrm{nm}} = 0.264$). Equilibrium temperature plotted versus laser intensity is shown in Fig. 7. We added a similar dependence for the solar spectrum ($\varepsilon_{\mathrm{Sun}} = 0.286$) without background (we neglect the 4-K space background radiation). The comparison of two profiles in this figure shows that the temperature of the grain in our experiment is similar to that expected near the Venus orbit.

An exponential dependence of the diffusion coefficient on the temperature means that this coefficient can differ by several orders of magnitude in different places of the space. The gas accumulated during a long time in the cold interstellar medium can then be quickly released near the Sun and change the mass composition of the pick-up ions.

The change of the diffusion coefficient with temperature influences strongly the amount of the gas that can be dissolved. Fig. 8 shows a computed maximum of the dissolved mass as a function of the N/D ratio for the sputtering yield, $Y = 1$. The dashed line neglects the grain sputtering, and it rises without limitations, whereas the full line exhibits a clear saturation that results from the fact that the grain is sputtered off earlier than the diffusion established an equilibrium density profile of the dissolved gas. However, we should point out that the results for large portions of the dissolved gas should be taken with care because our computation does not include structural changes of the grain that occur due to implantation of ions.

VI. Conclusion

We have presented the measurements of the diffusion of Ar atoms that were implanted into the amorphous carbon grain. This measurement was compared with theoretically obtained solutions of the diffusion equation. Our calculations show that the number of atoms that can be dissolved in a particular grain is directly proportional to its mass and inversely proportional to the diffusion coefficient of a given ion in the grain material. The time needed to reach this saturation level increases with the grain dimensions and decreases with the diffusion coefficient. Under our laboratory conditions, the maximum amount of the dissolved gas is as high as 2.2% of the grain mass, and this equilibrium density would be reached in ≈ 1000 h if the grain sputtering is neglected. On the other hand, the sputtering would completely destroy the grain in a comparable time. Since the diffusion coefficient strongly increases with temperature whereas the sputtering rate does not, the grain radiation budget should be taken into account in all considerations.

Acknowledgment

The authors would like to thank Prof. Vítek for endless discussions.

References

[1] I. Mann, H. Kimura, D. A. Biesecker, B. T. Tsurutani, E. Grün, R. B. McKibben, J.-C. Liou, R. M. MacQueen, T. Mukai, M. Guhathakurta, and P. Lamy, "Dust near the sun," *Space Sci. Rev.*, vol. 110, no. 3/4, pp. 269–305, Jan. 2004.

[2] I. Mann, "Interplanetary medium—A dusty plasma," *Adv. Space Res.*, vol. 41, no. 1, pp. 160–167, 2008.

[3] T. Minato, M. Köhler, H. Kimura, I. Mann, and T. Yamamoto, "Momentum transfer to interplanetary dust from the solar wind," *Astron. Astrophys.*, vol. 424, no. 2, pp. L13–L16, Sep. 2004.

[4] P. M. Banks, "Interplanetary hydrogen and helium from cosmic dust and the solar wind," *J. Geophys. Res.*, vol. 76, no. 19, pp. 4341–4348, Jan. 1971.

[5] R. S. Rajan, D. E. Brownlee, D. Tomandl, P. W. Hodge, H. Farrar, and R. A. Britten, "Detection of 4He in stratospheric particles gives evidence of extraterrestrial rigin," *Nature*, vol. 267, no. 5607, pp. 133–134, May 1977.

[6] A. O. Nier, "Helium and Neon in interplanetary dust particles," in *Analysis of Interplanetary Dust Particles*, vol. 310, E. Zolensky, T. L. Wilson, F. J. M. Rietmeijer, and G. J. Flynn, Eds. College Park, MD: AIP, 1994, ser. American Institute of Physics Conference Series, pp. 115–126.

[7] H. J. Fahr, H. W. Ripken, and G. Lay, "Plasma-dust interactions in the solar vicinity and their observational consequences," *Astron. Astrophys.*, vol. 102, no. 3, pp. 359–370, Oct. 1981.

[8] M. Gruntman, "H_2^+ pickup ions in the solar wind: Outgassing of interplanetary dust," *J. Geophys. Res.*, vol. 101, no. A7, pp. 15 555–15 568, Jul. 1996.

[9] P. Vernazza, R. P. Binzel, A. Rossi, M. Fulchignoni, and M. Birlan, "Solar wind as the origin of rapid reddening of asteroid surfaces," *Nature*, vol. 458, no. 7241, pp. 993–995, Apr. 2009.

[10] C. Plainaki, A. Milillo, S. Orsini, A. Mura, E. de Angelis, A. M. di Lellis, E. Dotto, S. Livi, V. Mangano, S. Massetti, and M. E. Palumbo, "Space weathering on near-Earth objects investigated by neutral-particle detection," *Planet. Space Sci.*, vol. 57, no. 3, pp. 384–392, Mar. 2009.

[11] L. V. Starukhina, "Polar regions of the moon as a potential repository of solar-wind-implanted gases," *Adv. Space Res.*, vol. 37, no. 1, pp. 50–58, 2006.

[12] G. Federici and C. Skinner, "Nuclear fusion research: Understanding plasma-surface interactions," in *Tritium Inventory in the Materials of the ITER Plasma-Facing Components*, vol. 78, *Chemical Physics*. Berlin, Germany: Springer-Verlag, Jan. 2006, ch. 12, pp. 287–317.

[13] H. Yoshida, M. Taniguchi, K. Yokoyama, Y. Yamauchi, Y. Hirohata, M. Akiba, and T. Hino, "Deuterium retention in carbon dust and

carbon–tungsten mixed dust prepared by deuterium arc discharge," *J. Nucl. Mater.*, vol. 329–333, pt. 1, pp. 790–794, Aug. 2004.
[14] P. Shukla and N. Tsintsadze, "Charged dust grain acceleration in tokamak edges," *Phys. Lett. A*, vol. 372, no. 12, pp. 2053–2055, Mar. 2008.
[15] D. Rudakov, W. West, C. Wong, N. Brooks, T. Evans, M. Fenstermacher, M. Groth, S. Krasheninnikov, C. Lasnier, A. McLean, A. Pigarov, W. Solomon, G. Antar, J. Boedo, R. Doerner, E. Hollmann, A. Hyatt, R. Moyer, and J. Watkins, "Migration of artificially introduced micron-size carbon dust in the DIII-D divertor," *J. Nucl. Mater.*, vol. 363–365, pp. 227–232, Jun. 2007.
[16] R. D. Kolasinski, J. E. Polk, D. Goebel, and L. K. Johnson, "Carbon sputtering yield measurements at grazing incidence," *Appl. Surf. Sci.*, vol. 254, no. 8, pp. 2506–2515, Feb. 2008.
[17] I. Čermák, "Laboruntersuchung elektrischer Aufladung kleiner Staubteilchen," Ph.D. dissertation, Naturwissenschaftlich-Mathematischen Gesamtfakultät, Ruprecht-Karls-Universität, Heidelberg, Germany, Nov. 1994.
[18] P. Žilavý, Z. Sternovský, I. Čermák, Z. Němeček, and J. Šafránková, "Surface potential of small particles charged by the medium-energy electron beam," *Vacuum*, vol. 50, no. 1/2, pp. 139–142, May/Jun. 1998.
[19] J. Pavlů, A. Velyhan, I. Richterová, Z. Němeček, J. Šafránková, I. Čermák, and P. Žilavý, "Mass-loss rate for MF resin microspheres," *IEEE Trans. Plasma Sci.*, vol. 32, no. 2, pp. 704–708, Apr. 2004.
[20] M. Jeřáb, I. Richterová, J. Pavlů, J. Šafránková, and Z. Němeček, "Influence of charging conditions on field ion emission from dust grains," *IEEE Trans. Plasma Sci.*, vol. 35, no. 2, pp. 292–296, Apr. 2007.
[21] J. F. Ziegler, J. P. Biersack, and M. D. Ziegler, *SRIM*, 2009. ver. 2008.04. [Online]. Available: http://www.srim.org
[22] J. F. Ziegler, J. P. Biersack, and M. D. Ziegler, *SRIM—The Stopping and Range of Ions in Matter*. Morrisville, NC: Lulu Press Co., 2008.
[23] M. Vyšinka, J. Vaverka, J. Pavlů, Z. Němeček, and J. Šafránková, "Depth profiles of ions implanted into spherical dust grains—A trim based model," in *Proc. Contrib. Papers, Part II—Phys. Plasmas Ionized Media WDS*, J. Šafránková and J. Pavlů, Eds., 2009, pp. 195–201.
[24] R. Behrisch and W. Eckstein, *Sputtering by Particle Bombardment*, vol. 110, R. Behrisch and W. Eckstein, Eds. Berlin, Germany: Springer-Verlag, 2007, ser. Topics in Applied Physics.
[25] P. Laven, "Effects of refractive index on glories," *Appl. Opt.*, vol. 47, no. 34, pp. H133–H142, Dec. 2008.
[26] P. Laven, *MiePlot*, 2009. v4. [Online]. Available: http://www.philiplaven.com/mieplot.htm
[27] C. Jager, H. Mutschke, and T. Henning, "Optical properties of carbonaceous dust analogues," *Astron. Astrophys.*, vol. 332, pp. 291–299, Apr. 1998.
[28] M. W. Williams and E. T. Arakawa, "Optical properties of glassy carbon from 0 to 82 eV," *J. Appl. Phys.*, vol. 43, no. 8, pp. 3460–3463, Aug. 1972.

Martin Beránek was born in Prague, Czech Republic, in 1983. He received the M.S. degree from Charles University, Prague, in 2007, where he is currently working toward the Ph.D. degree in the Department of Surface and Plasma Science, Faculty of Mathematics and Physics.

Marek Vyšinka was born in Brno, Czech Republic, in 1984. He received the M.S. degree from Charles University, Prague, Czech Republic, in 2008, where he is currently working toward the Ph.D. degree in the Department of Surface and Plasma Science, Faculty of Mathematics and Physics.

His recent research interest includes the laboratory simulation of elementary processes in dusty plasmas.

Jiří Pavlů was born in Pardubice, Czech Republic, in 1977. He received the M.S. and Ph.D. degrees from Charles University, Prague, Czech Republic, in 2001 and 2005, respectively.

Currently, he is a Senior Assistant with the Space Physics Laboratory, Department of Surface and Plasma Science, Faculty of Mathematics and Physics, Charles University. His research interests include the laboratory investigations of elementary processes on dust grains induced by electron, ion, and photon irradiations.

Ivana Richterová was born in Český Brod, Czech Republic, in 1979. She received the M.S. degree from Charles University, Prague, Czech Republic, in 2003, where she is currently working toward the Ph.D. degree in the Space Physics Laboratory, Department of Surface and Plasma Science, Faculty of Mathematics and Physics.

Her research is devoted to the laboratory investigation and modeling of elementary charging processes on dust grains.

Zdeněk Němeček was born in Prague, Czech Republic, in 1947. He received the M.S., Ph.D., and Dr.Sc. degrees from Charles University, Prague, in 1971, 1982, and 1996, respectively.

Since 1971, he has been holding several positions with the Faculty of Mathematics and Physics, Charles University, where he currently serves as the Dean. His research interests include the solar-wind interaction with the Earth's magnetosphere and the laboratory simulations of plasma processes.

Jana Šafránková was born in Teplice, Czech Republic, in 1947. She received the M.S., Ph.D., and Dr.Sc. degrees from Charles University, Prague, Czech Republic, in 1972, 1982, and 1996, respectively.

Since 1971, she has been holding several positions with the Faculty of Mathematics and Physics, Charles University, where she is currently the Director of the Department of Surface and Plasma Science and the Head of the Space Physics Laboratory. Her recent research interests include the magnetospheric physics and laboratory simulation of elementary processes in dusty plasmas.

Příloha A2.

Vyšinka, *M.,* Vaverka, *J.,* Pavlů, *J.,* Němeček, *Z.,* *a* Šafránková, *J., Depth Profiles of Ions Implanted into Spherical Dust Grains—a TRIM Based Model. In:* Safrankova, *J. a* Pavlu, *J. (Eds.)* WDS'09 Proceedings of Contributed Papers: Part II - Physics of Plasmas and Ionized Media*, Prague, Matfyzpress, 2009, pp. 195–201. ISBN 978-80-7378-102-6.*

WDS'09 Proceedings of Contributed Papers, Part II, 195–201, 2009. ISBN 978-80-7378-102-6 © MATFYZPRESS

Depth Profiles of Ions Implanted into Spherical Dust Grains—a TRIM Based Model

M. Vyšinka, J. Vaverka, J. Pavlů, Z. Němeček, and J. Šafránková

Charles University, Faculty of Mathematics and Physics, Prague, Czech Republic.

Abstract. Dust in the space and in laboratory experiments is often exposed to energetic ions. During this process, the ions are implanted into the grain. The grain can collect a significant charge that is spontaneously released due to ion field emission. To support the results of laboratory experiments on ion field emission, we adapted a TRIM-code (developed originally for a study of planar surfaces) on rotating spherical dust grains. This model modification was verified on glassy carbon grains. The results indicate that the peak of distribution of implanted ions is closer to the surface of spherical grains than in planar samples in the case of a normal angle of incidence. The output of the implantation model should serve as an input of the diffusion model and, finally, it will be implemented into the model of the ion field emission.

Introduction

Dust can be found in many environments ranging from the Earth (microchip manufacturing, dust in the atmosphere, etc.) to the space (surface of cosmic bodies, interplanetary matter, nebulae, etc.). In such environments, dust grains can be easily charged and their charge than significantly affects a grain motion as it can be seen, e.g., in plasma crystals [*Fortov et al.*, 2005], in spokes in Saturn s rings [*Mitchel et al.*, 2006] or in dust storms [*Renno and Kok*, 2008].

One of the charging mechanisms is ion attachment and corresponding discharging mechanism (at a high electric field intensity) is field ion emission. The field ion emission consists of three basic processes:

- field ionization (ionization of atoms from the surrounding atmosphere),
- field desorption (ionization of atoms adsorbed on a surface),
- field evaporation (ionization of atoms of the bulk material),

which differ particularly in a source of atoms that are ionized. We suggest that the field desorption should be considered in a broader context that includes the implantation of energetic ions into the bulk material. Implanted neutralized ions are driven toward the surface (and deeper into the dust grain) by diffusion. The diffusing atoms reaching the surface can be released from the dust grain as neutral atoms (at a low electric field intensity) or as ions (at a high electric field intensity – above 10^8 V/m). This process can be identified as a mass loss during mass measurements [*Beránek et al.*, 2010] or in discharging curves (during field ion emission experiments) [*Jeřáb et al.*, 2007] because shapes of these curves should depend, among others, on a depth profile of implanted ions. Thus, as a part of the field ion emission study, we developed a simple model computing implantation profiles of spherical dust grains.

As there are few models computing implantation range (e.g., [*Robinson and Torrens*, 1974],[*Yamamura and Mizuno*, 1985]), we base our model on a TRIM code which is widely used for studies of ion implantation [*Arkush et al.*, 2000] and target sputtering [*May et al.*, 2000]. The TRIM code is a part of a SRIM software package concerning the stopping and range of ions in matter. It is the Monte Carlo simulation of transport of ions through various targets (elementary/multi-component, one-layered/multi-layered, solid/gas, etc.) based on the theoretical models described in [*Ziegler et al.*, 1985]. Briefly, TRIM simulates the bombardment of a

planar target by projectiles of given kinetic energy and impact angle. The target is simulated as amorphous (i.e., given the density, the position of each atom inside the target is random). The depth inside the material at which the projectile hits a target atom is derived from interatomic potentials dependent on the colliding elements. If an atom in the target receives an energy larger than a given threshold, it will be able to escape from its position (the lattice site) and it will lose an amount of energy given by the bulk binding energy. Recoiling atoms may collide with other target atoms. TRIM follows the whole collision cascade. A depth of the ion penetration is given by the ion energy, electronic and nuclear stopping, and nuclear deflection. These three processes depend on target composition (and its properties) and ion species. For more details, see [*Ziegler et al.*, 2008].

Ion species, ion energy, angle of incidence, target material, target density, width and target binding energies (displacement energy, surface and lattice binding energies) serve as the TRIM input. This model was applied in many papers (see e.g., [*Bianchi and Ferrara*, 2005], [*May et al.*, 2000], and many others) on processes connected with the ion bombardment of dust grains but none of them reflected the shape effects because the TRIM simulation is developed for planar targets only.

TRIM Modification

The core of our modification deals with approximation of the spherical shape of the surface. The sphere is treated as a regular polyhedron and the number of faces is a free parameter of our model. We expect that the polyhedron is rotating in the parallel ion beam and thus the incidence angle, α changes accordingly. The computation methodic of as well as the broad discussion of errors resulting from our approximation are subjects of the following paragraphs and Figures 1 and 2.

We compute the implantation profile from 0° (normal incidence) to 90° (parallel incidence) of the incident angle with a given angular step (α). The resulting depth profile represents a histogram with the bin width of 1 Å. Finally, we sum all such histograms together with a certain weight. This process is illustrated in Figure 1.

Using TRIM, we obtain the depth profile for the i th angular step:

$$P_{i\,j} = \frac{x_j}{N} \tag{1}$$

where x_j is the number of ions in j th bin and N is the number of impinging ions. Assuming the grain rotation in a parallel ion beam, the weight of i th histogram is given by the surface area (S_i) related to the i th angular step (as it is shown in Figure 2). The weighted histogram is then given by:

$$P_i^{weighted} = P_i \frac{S_i}{S} \tag{2}$$

where S is the surface area of cross-section of the grain ($S = \pi R^2$). For zero angle, we have

$$S_0 = \pi R^2 sin(\frac{\alpha}{2}) \tag{3}$$

and for all subsequent angles

$$S_i = \pi R^2 \left(\sin^2 \left(\frac{2i+1}{2}\alpha \right) - \sin^2 \left(\frac{2i-1}{2}\alpha \right) \right) \tag{4}$$

The final implantation profile, P is then given by

$$P = \frac{\sum_{i=0}^{n} P_i S_i}{S} = P_0 \sin^2 \left(\frac{\alpha}{2} \right) + \sum_{i=1}^{n} P_i \left[\sin^2 \left(\frac{2i+1}{2}\alpha \right) - \sin^2 \left(\frac{2i-1}{2}\alpha \right) \right] \tag{5}$$

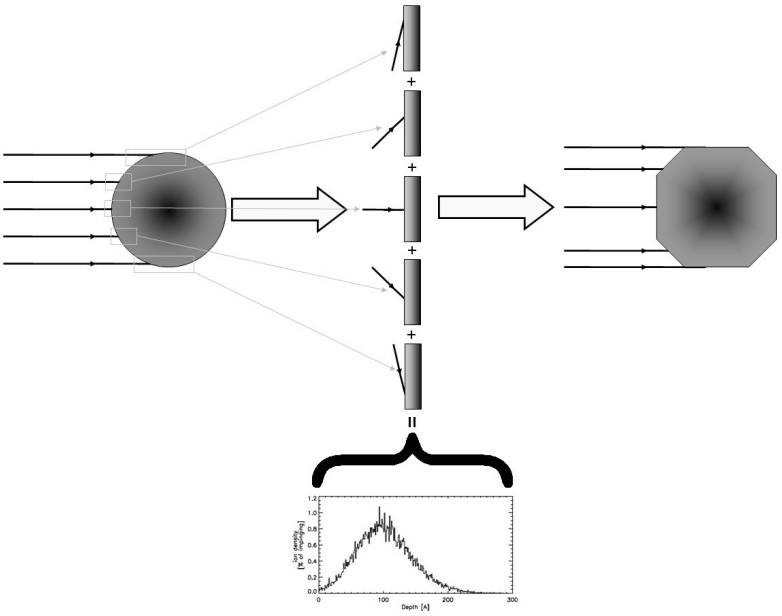

Figure 1. Illustration of the method. The spherical grain is substituted by a "polyhedron" grain (in this illustration with an angular step of 45°). The implantation profile is computed for every angle and all profiles are summed together. Edge effects are neglected, only depth profiles are computed (another directions are not taken into account).

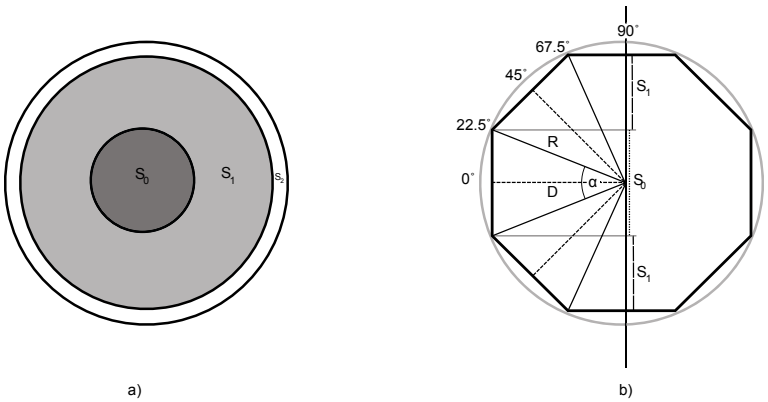

Figure 2. Every angle contributes to the final implantation profile according to the area corresponding to this angle. a) Front view, b) side view with geometry for $\alpha = 45°$ (R – radius of the grain). The surface area S_2 in the panel a) is neglected in the model that gives raise an error described in the text.

where $n = \frac{90}{\alpha} - 1$ (note that the equation (5) expects that n is an integer and it limits a selection of the angular step, α). We are neglecting the last angular step (for parallel incidence) that introduces some error in the results. This error arises with the difference between R and D (Figure 2 right) and scales up as $1 - \cos\left(\frac{\alpha}{2}\right)$ or $1 - \cos^2\left(\frac{\alpha}{2}\right)$ for the diameter and surface area errors, respectively. For the 5° angular step, the error is $\approx 1 \times 10^{-3}$ ($\approx 2 \times 10^{-3}$ for the surface error) that is in the TRIM accuracy limit. The effect of this error can be later seen in Figure 5.

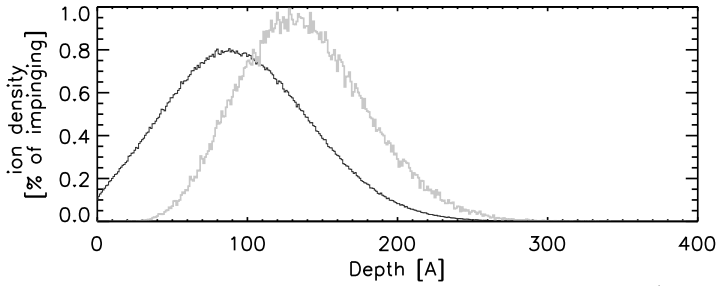

Figure 3. Comparison of the implantation profiles obtained by our model (thin black line) and normal incidence ion beam (thick grey line) for 7 keV argon impinging onto the glassy carbon grain (density 1.54 g/cm^3), 10^4 ions, the model with an angular step of 5°).

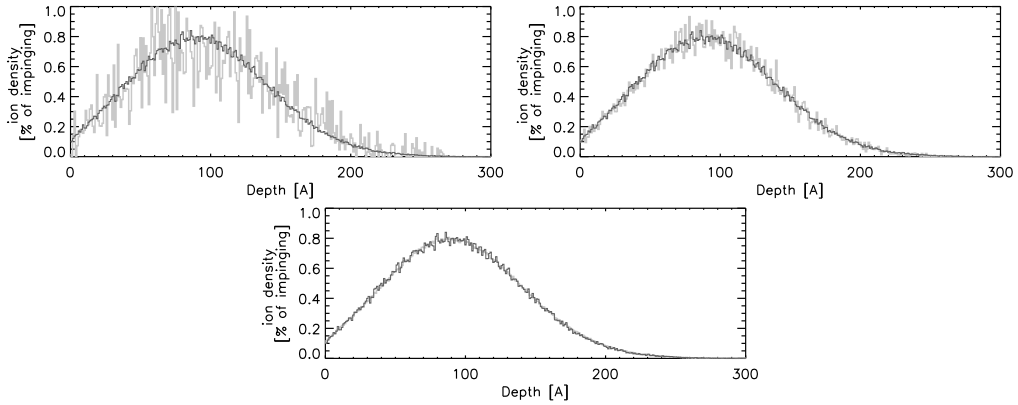

Figure 4. Comparison of implantation profiles for various numbers of ions. The thin black line is for 10^4 ions in all figures. The thick gray lines are for 10^2 (upper left), 10^3 (upper right) and 10^5 (bottom) ions, respectively.

Results

The depth profiles of implanted ions in spherical grains should differ from that in planar samples at any incidence angle because ions impinge the grain with all incidence angles simultaneously. A comparison of our model and the normal incidence ion beam is depicted in Figure 3.

Implantation depth for ions under oblique incidence is smaller than for the normal incidence. This is the reason why the maximum of implanted ions in our model is closer to surface of the grain than for normal incidence.

To check how the chosen model inputs and parameters affect the resulting profiles, we run several simulations with different input conditions – various numbers of impinging ions, angular steps, target densities, and ion energies. A standard setting was: ions – argon, 7 keV, 10^4 ions, 5° angular step; target – carbon, density 1.54 g/cm^3 (glassy carbon), displacement energy 28 eV, surface binding energy 7.43 eV, and lattice binding energy 3 eV (default values in TRIM).

Figure 4 shows comparisons of implantation profiles for various numbers of impinging ions ranging from 10^2 to 10^5 ions. A better statistics and smoother implantation profile need to use more ions, but, on the other hand, many ions slow down the simulations. In Figure 4 bottom, we can see that 10^4 ions represent a reasonable number of ions and a relatively short computation time (in the range of minutes per angular step for a standard PC).

Comparisons of implantation profiles for various angular steps in the range of 45° – 0 5°

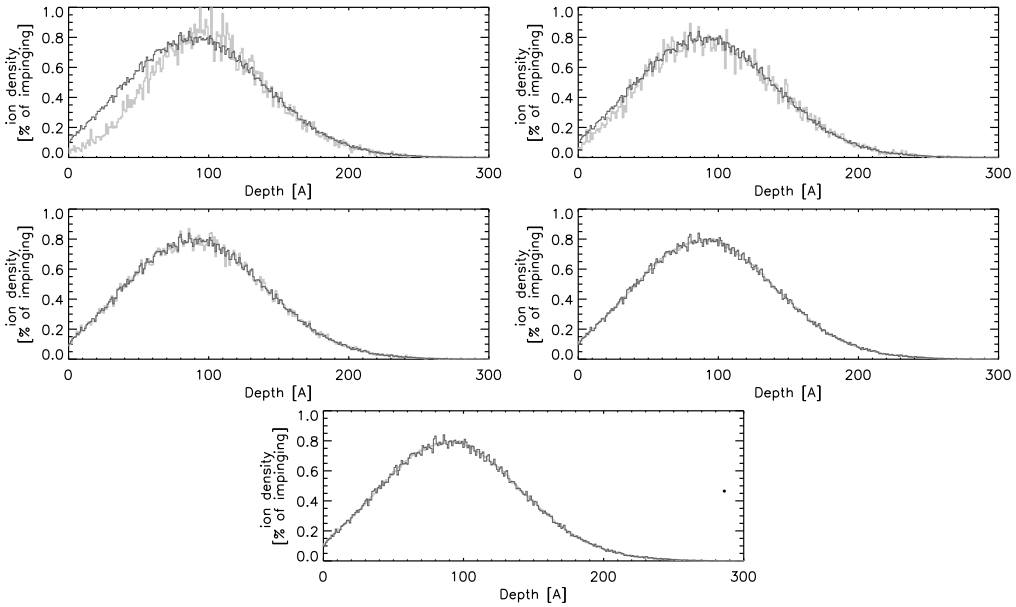

Figure 5. Comparison of implantation profiles for various angular steps. The thin black line is for the 5° angular step in all figures. The thick gray lines are for 45° (upper left), 30° (upper right), 10° (middle left), 1° (middle right) and 0 5° (bottom) angular steps, respectively.

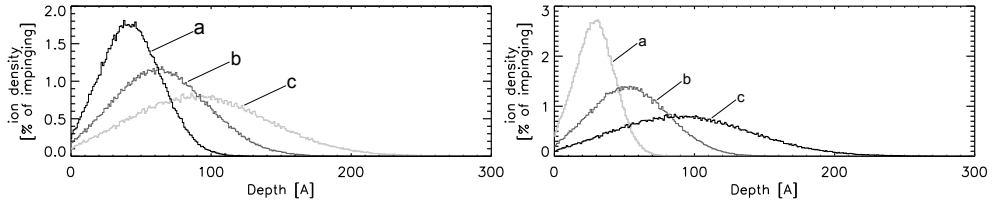

Figure 6. Comparison of the implantation profiles for various target densities: a – 3.5 g/cm^3 (diamond), b – 2.253 g/cm^3 (graphite), c – 1.54 g/cm^3 (glassy carbon) with 7 keV ion beam energy (left) and various ion beam energies: a – 1 keV, b – 3 keV, c – 7 keV with density 1.54 g/cm^3.

are plotted in Figure 5. It is evident that the 5° angular step is good enough for a reasonable sphericity and a relatively short computation time. It should be mentioned that refinement of the angular step is combined with the increasing number of ions, i.e., when certain amount of ions for every angle is used, more angles mean more ions.

In Figure 6 left, comparisons of implantation profiles for targets with various densities are shown. In our laboratory experiments [*Vaverka et al.*, 2009], we are using the glassy carbon dust with density of 1.54 g/cm^3, but carbon exists in many modifications with different densities. The most common is graphite (2.253 g/cm^3) and the densest one is diamond (3.5 g/cm^3). The density, even in this relatively small range, has a significant effect on the implantation profile. It should be stressed out here that this effect is only due to the density, as TRIM does not account for a crystal structure. In Figure 6 right, comparisons of implantation profiles for various ion energies (1, 3 and 7 keV) are displayed. One can note the significant change of the depth profile with the ion energy, that is important in our charging experiment. The dust grain potential reaches charges very quickly the surface potential around 6 kV under bombardment of the 7 keV Ar^+ beam (if the charge is not compensated by the electron beam) and thus the relative energy is only about 1 keV for most of impinging ions.

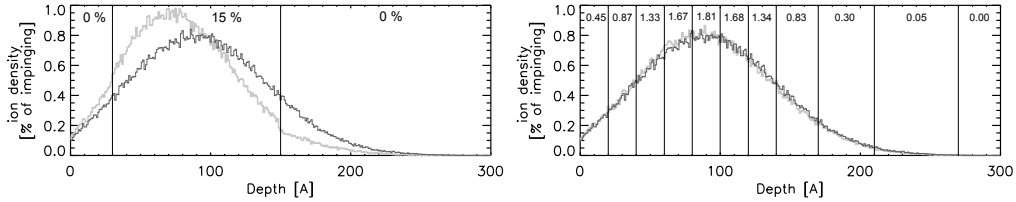

Figure 7. Comparison of implantation profiles for damaged and undamaged dust grains. The black curves are for the undamaged grain (no implanted argon) and the gray curves are for damaged grains (left: 3-layer model, right: 11-layer model). The numbers above the graphs are percentages of argon in a given layer.

The last studied effect is the influence of implanted ions on the implantation profile. TRIM cannot calculate with target damaged by the implanted ions, but these ions could change a local density in the dust grain and, as it can be seen in Figure 6 left, the density significantly affects the implantation profile.

Figure 7 shows comparisons of implantation profiles for targets with various amount of implanted argon. In the left panel, there is a model with 3 layers (0–30 Å without argon, 30–150 Å with 15 % of argon and from 150 Å without argon). From this panel we can see that implanted ions could influence the implantation profile, but the amount of argon is unreasonable high. In the right panel, there is a similar model consisting of 11 layers with amount of argon based on the simulated profile for dust grain without argon and a rough estimation of total argon amount from the experiment [*Beránek et al.*, 2010]. The difference in implantation profiles between the dust grain without argon (black curve) and dust grain with implanted argon (gray curve) can be hardly seen.

Discussion

Our model based on the TRIM code contains two main parameters: the number of ions and the angular step. These parameters have a similar effect; the increasing number of ions improves statistics and reduces noise in the depth profile histogram, but, on the other hand, it extends the simulation time and memory requirements. From Figure 4, it can be seen that 10^4 ions is sufficient number to know the shape of the depth profile. Refinement of the angular step also reduces noise in histograms of the implantation profile and extends the simulation time. The shape of the depth profile does not change from the 5° (and finer) angular step (Figure 5), so this value is also sufficient for our simulations. It should be mentioned that the refinement of the angular step is combined with the increasing number of ions, i.e., when certain amount of ions for every angle is used, more angles mean more ions. The implantation profile depends on the ion beam energy and target density. The similarity of these dependences that can be seen in Figure 6 left and right is only accidental (differences are in the height and width of profiles). Implanted ions can affect the dust grain properties via the density change, but we do not implant enough ions to affect the shape of the implantation profile (Figure 7) in our experimental conditions.

Implantation profiles are calculated under assumption that dust grains are bombarded by ions uniformly. That implies a rotation of the dust grain. We do not know the grain rotational state but we can expect this due to the dust charge–beam interaction and we can thus expect that each angle contributes to the final implantation profile according to its surface area (Figure 2).

These results are valid for an absolute flat surface. Scanning electron microscopy allows to check the shape of the real dust grain in the μm range but we are unable to check the surface shape in the nm range in which these phenomena occur. The surface roughness can significantly affect the implantation profile, more implanted ions would be closer to the surface.

Conclusion

We developed a model for computation of the implantation profiles of ions in spherical dust grains. These profiles are in the range of several tens of nanometers (for carbon target and 7 keV argon ions) and their shapes and deepness depend strongly on the ion beam energy and target density. For our purposes, sufficient parameters of our model are 5° of the angular step and 10^4 impinging ions per one angular step. The computed implantation profile will be an input of the future diffusion model, which should be able to explain some properties of the dust grain discharging via ion field emission.

Acknowledgments. The authors would like to express their appreciation for the supports to the Charles University Grant Agency under Contract No. 146207 and to the Czech Science Foundation under Contract 202/08/0063.

References

Arkush, R., M.H. Mintz, and N. Shamir, Passivation of Uranium towards Air corrosion by N_2^+ and C^+ ion implantation, *J. Nucl. Mater.*, 281, 182–190 (2000).

Beránek, M., M. Vyšinka, I. Richterová, J. Pavlů, Z. Němeček, and J. Šafránková, Dust as a gas carrier, *IEEE Trans. Plasma Sci.*, submitted (2010).

Bianchi, S., and A. Ferrara, Intergalactic Medium Metal Enrichment through Dust Sputtering, *Mon. Not. R. Astron. Soc.* 358, 379–396 (2005).

Jeřáb, M., I. Richterová, J. Pavlů, J. Šafránková, and Z. Němeček, Influence of Charging Conditions on Field Ion Emission from Dust Grains, *IEEE Trans. Plasma Sci.* 35, 292–296 (2007).

Fortov, V.E., A.V. Ivlev, S.A. Khrapak, and G.E. Morfill, Complex (dusty) plasmas: Current status, open issues, perspectives, *Phys. Reports*, 421, 1–103 (2005).

May, P.V., G. Pineau des Forets, D.R. Flower, D. Field, N.L. Allan, and J.A. Purton, Sputtering of grains in C-type shocks, *Mon. Not. R. Astron. Soc.* 318, 809–816 (2000).

Mitchell, C.J., M. Horányi, O. Havnes, and C.C. Porco, Saturn s Spokes: Lost and Found, *Science* 311, 1587–1589 (2006).

Renno, N.O., and J.F. Kok, Electrical Activity and Dust Lifting on Earth, Mars and Beyond, *Space Sci. Rev.* 137, 419–434 (2008).

Robinson, M.T., and I.M. Torrens, Computer Simulation of Atomic-Displacement Cascades in Solids in the Binary-Collision Approximation, *Phys. Rev. B* 9, 5008–5024 (1974).

Yamamura, Y., and Y. Mizuno, Report No. IPPJ-AM-40,*Institute of Plasma Physics, Nagoya University* (1985).

Vaverka, J., M. Vyšinka, J. Pavlů, M. Beránek, J. Šafránková, and Z. Němeček, Ion Field Emission from Micron-sized Dust Grains, in *WDS'09 Proceedings of Contributed Papers: Part II—Physics of Plasmas and Ionized Media* (eds. J. Šafránková and J. Pavlů), Prague, Matfyzpress (2009), this issue.

Ziegler, J.F., J.P. Biersack, and U. Littmark, Stopping Powers and Ranges of Ions in Matter, New York, Pergamon (1985), pp. 25ff.

Ziegler, J.F., J.P. Biersack, and M.D. Ziegler, SRIM The Stopping and Range of Ions in Matter, ISBN 0-9654207-1-X (2008).

Příloha A3.

Vyšinka, *M.*, Němeček, *Z.*, Šafránková, *J.*, Pavlů, *J.*, Vaverka, *J.*, *a* Lavková, *J.*, *Sputtering of Spherical SiO_2 Samples.* IEEE Trans. Plasma Sci., *2016*, **44***(6), 1036–1044. DOI 10.1109/TPS.2016.2564502*

Sputtering of Spherical SiO_2 Samples

Marek Vyšinka, Zdeněk Němeček, Jana Šafránková, Jiří Pavlů, Jakub Vaverka, and Jaroslava Lavková

***Abstract*— Dust grains in the interplanetary environment can be basically found in two locations—floating in the free space or attached to a surface of asteroids, comets, or moons. They are sputtered by the impacts of energetic ions, and this process supplies the interplanetary space with heavy elements. The sputtering yield is generally estimated on the basis of laboratory investigations of planar samples. We use silica micrometer-sized spherical grains as a prototype of a space-borne dust, bombard them by 2-keV Ar ions, and monitor the influences of simultaneous application of the electron beam as well as the electric field at the dust surface on the sputtering yield. We found that the increase in the sputtering yield due to the electron impact is much larger than expected and it can enhance the sputtering yield by a factor of 1.6 in a comparison with the sole ion bombardment. On the other hand, the influence of the electric field is not so strong (if any) and it is masked by electron impacts in our experiment. Sputtering of the grains fixed at a surface by 30-keV Ga ions revealed that the angular profile of the yield is flatter than that frequently used for a description of the sputtering process. Finally, we compare these results with the published sputtering yield values.**

***Index Terms*— Dust charging, dusty plasmas, electron emission, sputtering.**

I. Introduction

ENERGETIC ions from the solar wind, local pick-up ions, or magnetospheric plasma ions impact the atmosphere and surfaces of solar system bodies [1]. These energetic incident ions deposit the energy in the surfaces of solid objects or surfaces, and it can lead to the ejection of atoms and molecules, a process referred to as sputtering.

The lunar surface is composed of rocks and regolith, i.e., soil-like layer with the grain sizes from centimeters to submicrometer scales [2]. The dust layer consists of a nonconducting material chemically composed from a mixture of oxides (mainly SiO_2 and Al_2O_3). Due to a lack of the significant atmosphere and strong magnetic field, both the dust laying on and levitating above the lunar surface are exposed to direct solar wind and magnetospheric plasma irradiation. This irradiation leads to sputtering of a surface material, but it represents only a minor contribution to the lunar exosphere [3]. Wurz *et al.* [4] found that it is responsible for 10^7 m^{-3}, but the experimentally determined total exospheric density is about 10^{12} m^{-3} and the main contributions are supposed to be thermodesorption and photodesorption of volatile elements. Sputtered atoms dominate in the lunar exosphere above 1000 km as they have velocities exceeding the escaping velocity from the lunar gravity field [4], [5].

The sputtering yield of individual grains (e.g., grains floating above the surface) is enhanced in a comparison with laboratory experiments for flat bulk targets (see [6], [7]); on the other hand, the sputtering yield is often reduced due to recapturing of sputtering products in the cases of dust grains covering surfaces [8], [9].

With the presence of the highly charged ions, the sputtering yield is enhanced and nanodefects are produced on the surface. For the insulator, the sputtering yield linearly increases with the ion potential energy [10]. In the solar wind, except the proton component that represents about 93% of the charged particle flux, the remaining 7% is distributed among the major solar wind heavier ions (He through Ar [11]). These heavy elements in the solar wind are usually multicharged (e.g., O^{6+} and Fe^{10+}), thus their internal energy can enhance the sputtering yield of nonconducting grains by a potential sputtering mechanism [11]–[13]. This potential sputtering may significantly alter the total sputtering yield (e.g., of the lunar surface oxides) despite their low abundances relative to protons [4], [14]. When both kinetic and potential sputterings are taken into account, Barghouty *et al.* [11] reported that heavy ions contribute to the lunar regolith sputtering by 26% without the potential sputtering and by 52% including that.

Hijazi *et al.* [15] reported sputtering of the anorthite-like material as a representative of soils found in the lunar highlands. This material was impacted by singly and multicharged ions corresponding to solar wind ions (protons, as well as singly and multicharged Ar ions as proxies for the nonreactive heavy solar wind constituents in the charge state from $+1$ to $+9$). Their results show a yield increase by a factor of about 80 for Ar^+ versus H^+ and an enhancement by a factor of 1.67 between Ar^{9+} and Ar^+ that can be an indication of a potential sputtering effect.

Dust in the space is simultaneously bombarded by ions and electrons, and electron-stimulated desorption can enhance the sputtering rate. This effect was investigated by Yakabe *et al.* [16] on SiO_2 planar targets and they found about linearly increasing sputtering rate with the electron current flowing on the surface. The investigations were motivated by applications in the Auger spectroscopy and thus used electron current densities were rather high, up to 150 A/m^2, whereas solar wind electrons can provide only several mA/m^2 and the currents in the magnetosphere are even lower.

Manuscript received August 28, 2015; revised November 23, 2015, February 3, 2016, and March 11, 2016; accepted May 2, 2016. Date of current version June 8, 2016. This work was supported in part by the Czech Science Foundation under Project 16-05762S and Project P209/11/1412 and in part by the Grant Agency of the Charles University under Project 1410213.

The authors are with the Faculty of Mathematics and Physics, Charles University in Prague, Prague 18000, Czech Republic (e-mail: vysinkam@seznam.cz; zdenek.nemecek@mff.cuni.cz; jana.safrankova@mff.cuni.cz; jiri.pavlu@mff.cuni.cz; jakubvaverka@gmail.com; alfa88@azet.sk).

Color versions of one or more of the figures in this paper are available online at http://ieeexplore.ieee.org.

Digital Object Identifier 10.1109/TPS.2016.2564502

The sputtering yield strongly depends on the incidence angle having maximum at 70–80°, and this dependence is especially important for dust grains. However, experimental data on the yield angular dependence are rather sparse, namely, for oxides and compounds (see [17] for a review). Researchers usually rely on simulated dependences (see [6], [13], [18]), and the TRIM software package [19], [20] is frequently used for this purpose (see [21]). However, modeling approaches need knowledge of input parameters that are quite disputable for multicomponent targets.

Nietiadi *et al.* [21] used Monte Carlo simulations for the determination of the dependence of the sputtering yield of spherical Si samples on their size. They found the enhanced yield if a penetration depth of primary ions into the target material was comparable with the target radius. However, this effect would be negligible for micrometer-sized samples used in this paper.

In this paper, we have carried out two different experiments:

1) sputtering of SiO_2 spherically shaped grains levitating in the free space by a 2-keV Ar ion beam;
2) sputtering of the same dust prototypes placed on a surface and influenced by an intense 30-keV Ga ion beam.

The aims of these experiments are to test the hypothesis about an influence of the electric field at the dust grain surface on the sputtering yield [22] and to determine an angular dependence of the sputtering yield. We can conclude that although our results are in a general agreement with already known values and angular profiles of the sputtering yield for a pure ion impact, a simultaneous electron bombardment can enhance the sputtering yield by a factor of 1.6, whereas the expected dependence of the yield on the surface electric field was not found. The experiment with the grains fixed at the surface revealed that the frequently used angular profile of the sputtering yield would be corrected.

II. Experiments With a Levitating Dust Grain

The experiment on sputtering of a levitating dust grain uses the electrodynamic quadrupole trap inside an ultra-high vacuum chamber [23]–[25]. The initially charged dust grain is trapped, and the frequency of its oscillations within the trap is recorded. This frequency is directly proportional to charge-to-mass ratio, Q/m, of the grain, and we use it for the determination of all quantities that are important for the description of the sputtering process.

1) The grain mass is calculated from a change of the oscillation frequency corresponding to the change of the grain charge by one electron (see [23] and the references therein).
2) The grain size is determined as the diameter of a sphere with the mass known from 1) using a specific mass of the silica grain from the manufacturer.
3) The grain surface potential is directly proportional to its charge. The proportionality constant is a grain capacitance that was calculated as the capacitance of a sphere with diameter from 2).
4) The ion flux impinging the grain was calculated from the ion beam current measured by the Faraday cup (FC). The grain is sputtered by a very small fraction of beam ions that depends on the position of the grain within the beam, on the beam spatial profile, and on the grain surface potential, ϕ. Since the grain is small and there is no sheath around it, we can use orbital motion limited approximation (see [26], [27]) and write the dependence of a number of ions falling onto the surface N_ϕ on the grain potential as

$$N_\phi = N_0 \cdot \left(1 - \frac{e \cdot \phi}{E_0}\right) \tag{1}$$

where N_0 is the number of impinging ions for the surface potential of the grain, $\phi = 0$, and E_0 is the energy of impinging ions.

The value of N_0 still depends on the beam size, its spatial profile, and the grain diameter. Since the ion source is equipped with the mass filter, only singly charged ions are in action. When such ions fall on the grain, they interact with the grain matter, recombine, and leave the grain as neutral atoms [28]. The sputtered products are also not charged, and a portion of electrons emitted by an ion impact with energies above 10 eV is smaller than $\approx 10^{-3}$ (see [29]). For these reasons, we can assume that the recorded change of the grain charge expressed in units of the elementary charge is approximately equal to the number of ions that have fallen onto the grain surface charged to the potential of 10 V or larger.

In order to determine a portion of ions falling onto the grain, we made a dynamic calibration. The ion gun is equipped with a fast sampling system allowing short (1–10 ms) shots. We have recorded a change of the grain charge, ΔQ, its potential, ϕ, and the integral of the beam current, J, during such shot. The ratio of $B(\phi) = \Delta Q/eJ$ (e is the elementary charge) can be considered as a proportionality constant between the integral of the beam current recorded by the FC and a number of ions impacted the grain during the shot for a given value of ϕ. A value, B_0, corresponding to $\phi = 0$ can be easily obtained from (1), and then $N_0 = B_0 \cdot J$. It should be noted that although we use the ion beam energies of 2 or 3 keV, a determination of B was carried out on only slightly charged grains ($\phi \approx 10$ V), and thus a correction on the grain potential was always lower than 1% in our experiment. Details on the calibration procedure can be found in [30]. This procedure was repeated several times prior to each sputtering session using shots of different durations, and a mean value of the calibration constant was used in further calculations. Moreover, the beam profile depends on the gun setting, and thus the calibration procedure was repeated after each change of the ion energy.

A. Sequence of Measurements

Measurements of the sputtering rate consist of several repeating steps.

1) The grain released from the dust dropper was initially charged to a low ($\approx$+7 V) potential by a 1-keV electron beam. Note that small SiO_2 spheres are charged

positively if the electron beam energy exceeds ≈100 eV because the secondary emission yield exceeds unity (see [24, Fig. 3] that uses the same samples). The electron impact causes a desorption of impurities present on the dust surface that lasts several minutes. This electron-stimulated desorption can lead to a decrease (usually nonmeasurable) of the grain mass, but even prolonged (≈20 h) further electron bombardment does not change the grain mass.

2) Measurements of the grain mass start with a decrease in the grain charge by low-energy electrons to about 100 of elementary charges. Such a low charge is needed for a reliable determination of the grain mass [23].
3) A determination of the calibration constant B_0 for the current ion gun setting.
4) Gradual increasing in an intensity of the ion beam of the preset energy. The electron beam can be in operation or it can be switched OFF, depending on the type of the experiment. The ion impact increases the grain charge, and it requires changes of the amplitude and frequency of the HV sources supplying the trap electrodes. All these changes should be slow and synchronized; otherwise, the grain is lost. The energy of the Ar ion beam was 2 keV for the sputtering experiment with simultaneous electron bombardment that keeps the grain potential at low values. This energy was increased for the experiments with decreased electron beam intensity to hold the energy of Ar ions impinging the grain at about 2 keV.
5) Keeping the energy and intensity of the ion beam and simultaneous recording of the grain Q/m ratio and FC current. This sputtering unit lasted usually ≈5 h; it was followed by the mass measurements (step 2), and the whole sequence was repeated until the grain was lost from the trap.

Pavlů *et al.* [22] used the same setup for sputtering of Au spherical grains and argued that these samples did not rotate and that the sputtering shaped them to an ellipsoid of revolution due to the angular dependence of the sputtering rate. However, the ions bring their charges to the front side of the grain. This charge is freely distributed along the conducting surface, but the dielectric grains are charged unevenly and the interaction of their dipole moment with the electric field of the ion beam would lead to their rotation and uniform bombardment. Consequently, the measured sputtering yield is averaged across all incident angles.

B. Sputtering Yield

The sputtering yield is usually defined for noncharged surfaces. Since the charged spherical grain defocusses the ion beam and decreases a number of ions falling onto its surface, the situation is more complicated in such a case. Let us assume that a number of ions falling onto a noncharged grain is N_0 and the corresponding number of sputtered atoms is n_0. The sputtering yield is defined as a ratio of n_0/N_0. Such yield would be measured for a conducting sphere attached to a grounded surface. If the grain is levitating in the beam of the same density, it is charged to a surface potential ϕ. The number of ions falling onto its surface decreases to N_ϕ [see (1)] and the number of material atoms expelled from the grain is marked as n_ϕ. The corresponding yield is then given by the ratio of n_ϕ/N_ϕ. Under assumption that the sputtering process does not depend on the grain potential, n_0/N_0 would be equal to n_ϕ/N_ϕ, but the influence of the grain potential is one of the subjects of this paper.

We use this sputtering yield definition throughout this paper, but we should note that the geometric definition of the yield of the charged sample, n_ϕ/N_0, is also plausible because the grain potential (and thus the N_ϕ value) may not be known in some cases, whereas N_0 can be obtained from the beam density and grain geometric cross section. This geometric yield is always equal to or lower than the true yield because the grain charge decreases the number of primary ions falling onto its surface.

The described sputtering experiment uses monodisperse SiO_2 spherical samples. In order to estimate a possible dependence of the sputtering yield on the electric field at the grain surface, three particular experiments differing by the grain charge were performed. As it is noted above, the grain charge (and surface potential) was controlled by the intensity of the 1-keV electron beam.

The first experiment used the grain with the initial mass of 1.190×10^{-15} kg that corresponds to a grain diameter of 1.01 μm. During 24 sputtering intervals with a total duration of 101 h, 8.34×10^{-16} kg of the grain material (i.e., ≈70% of the initial mass) was sputtered. The grain surface potential was kept at ≈10 V by the electron beam. An evolution of the grain mass that was measured at the beginning of each sputtering interval is shown in Fig. 1(a) as a function of time. Fig. 1 shows a gradual decrease of the mass-loss rate that was attributed to a gradually decreasing grain cross section. To estimate sputtering yield, we have calculated the cumulative ion dose impinging the grain with an account for the decreasing grain diameter.

The calculations of a partial ion dose that influenced the grain during i-th sputtering session proceeded as follows.

1) A determination of the calibration constant B_{0i} and the grain mass m_i. The value of B_{0i} includes the effect of the decreasing grain diameter due to the sputtering.
2) The value of the grain potential ϕ_i was calculated using the actual grain mass, diameter, and charge. It should be stressed out that the value of the potential is given by a balance of charging and discharging currents and all of them are proportional to the grain surface area, and thus this potential did not change notably from one to another session.
3) The integral of the FC current J_i over the session was recalculated to the partial dose, $N_{\phi i} = B_{0i}(1 - e \cdot \phi_i/E_0) \cdot J_i$. This recalculation accounts for a decrease of the affected grain surface caused by the repulsion of the beam ions.

The ion dose in Figs. 1 and 2 is a sum of these partial doses.

An evolution of the grain mass with the cumulative ion dose is demonstrated in Fig. 1(b). As it can be seen, this dependence can be fitted by a straight line with a very reasonable accuracy. The slope of this line is the sputtering

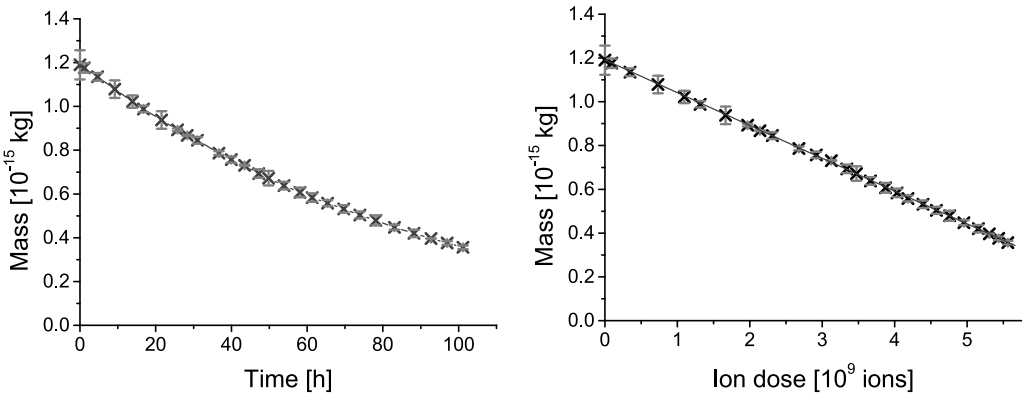

Fig. 1. (a) Temporal evolution of the grain mass during sputtering by 2-keV Ar ions and 1-keV electrons. (b) Dependence of the grain mass on the ion dose. The line in (b) shows a linear fit. Error bars are given by the errors of the mass measurements.

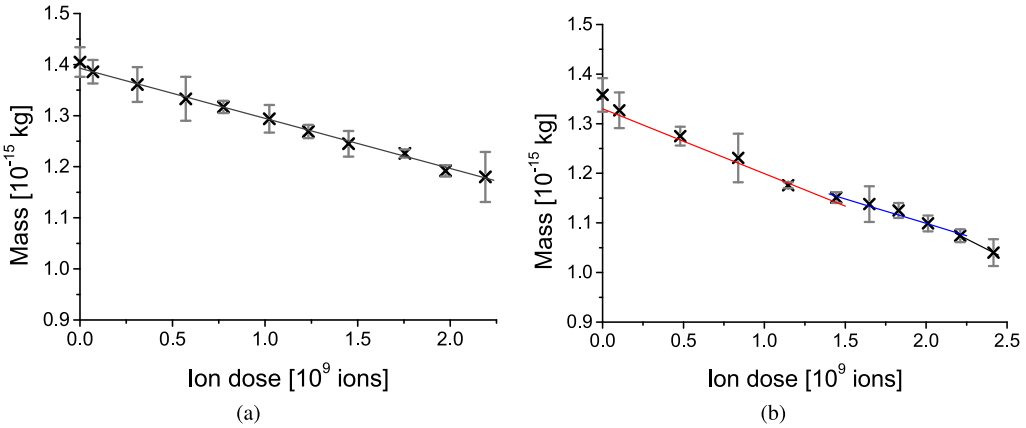

Fig. 2. Dependence of the grain mass on the number of impinging ions during sputtering at (a) high (1.3 kV) and (b) varying surface potentials: 0.8 kV—red line, 1.4 kV—blue line, and 9 V—black line. All lines represent linear fits of data points.

yield that was determined as $Y = (90.2 \pm 0.3)$ amu/ion $= (1.501 \pm 0.004)$ SiO_2/ion. The sputtering rate is usually given in numbers of molecules per incident ion, but the sputtering is not necessarily stoichiometric [31], [32], and thus the number of amu (atomic mass units) seems to be more informative.

The electron beam was switched OFF during the second experiment, and thus the grain surface potential reached $\approx$1.3 kV given by the field emission [33]. It corresponds to the electric field intensity of 1.7×10^9 V/m at the grain surface. The initial grain mass was 1.405×10^{-15} kg (diameter of 1.07 μm) at the beginning of the sputtering sequence, and about 16% of the mass was sputtered during 49 h of the ion bombardment. The grain mass as a function of the cumulative ion dose is shown in Fig. 2(a). Although an increase of the sputtering yield due to the high electric field at the grain surface was expected, the linear fit to the experimental points provides the value of $Y = (59 \pm 5)$ amu/ion $= (0.98 \pm 0.09)$ SiO_2/ion that is significantly lower than the yield determined for the uncharged sample.

Since the above experiments used two different samples, we carried out the third experiment with a new grain (mass 1.358×10^{-15} kg and diameter 1.06 μm). The grain was initially kept at 0.8 kV of the surface potential by the electron beam of low intensity, and four sputtering sequences of about 5 h of duration were realized. The electron beam was switched OFF for the next four sputtering sequences, and thus the grain potential was about 1.4 kV. The last sputtering sequence used the full intensity of the electron beam that kept the grain at about 10 V of the potential. The results of this experiment are shown in Fig. 2(b). Resulting sputtering yields determined from the linear fits shown in Fig. 2 are: 1) $Y = (78 \pm 11)$ amu/ion $= (1.3 \pm 0.2)$ SiO_2/ion for the surface potential of 0.8 kV; 2) $Y = (60 \pm 13)$ amu/ion $= (1.0 \pm 0.2)$ SiO_2/ion for the surface potential of 1.4 kV; and 3) $Y = 100$ amu/ion $= 1.66$ SiO_2/ion for the surface potential of 9 V. Note that these yields correspond to different energies of the impinging ions because the beam energy was set to 3 kV for all measurements. The experimental conditions and

TABLE I
OVERVIEW OF PARTICULAR EXPERIMENT CONDITIONS GIVEN IN THE FIGURES 1 AND 2

	Fig.	init. mass	ϕ	E_0	E_ϕ	duration	measured yield		SRIM yield	
		10^{-15} kg	kV	keV	keV	hours	amu/ion	SiO_2/ion	amu/ion	SiO_2/ion
1	1b	1.19	0.01	2	2	101	90.2 ± 0.3	1.501 ± 0.004	98	1.6
2	2a	1.41	1.3	3	1.7	49	59 ± 5	0.98 ± 0.09	90	1.5
3	2b	1.36	0.8	3	2.2	20	78 ± 11	1.3 ± 0.2	102	1.7
4	2b	1.15	1.4	3	1.6	20	60 ± 13	1 ± 0.2	88	1.5
5	2b	1.07	0.01	3	3	5	100	1.66	117	2

results are summarized in Table I. The rows correspond to particular experiments described above, and they are marked by references to Figs. 1 and 2 where the results of a particular experiment are shown. As it can be seen in Table I, the real ion impact energy, E_ϕ, varies from 1.6 to 3 keV in different experiments, and thus the observed changes of the yield can be (partly) caused by the energetic dependence of the sputtering yield. Uncertainties given in the yield column are uncertainties of linear fits shown in the corresponding figures, and they do not reflect the systematic uncertainties of the experimental method that can be hardly determined. We expect that a number of impinging ions is equal to the number of elementary charges that the grain gained during calibration shots and neglect a portion of energetic secondary electrons that would increase the positive charge of the grain. On the other hand, a very small number of outgoing species are ionized and this effect decreases the grain charge and these two effects partly compensate. We believe that the resulting error is of the order of 1%.

We have developed a routine that uses the SRIM software package [20] and allows us a computation of the yield from spherical samples bombarded by a parallel ion beam. The spherical grain was replaced by a polyhedron of revolution with a step of 1^o, and the sputtering yield was computed as a weighted sum of partial yields. The results of this computation are given in the last two columns of Table I. This procedure uses the real ion impact energy that is equal to $E_\phi = E_0 - e\phi$, but it still expects the parallel beam. If the grain is charged, the ion beam is defocused and the affected area of the grain decreases, but it can be easily shown that an angular distribution of the ions falling on the charged surface is conserved. The software computes probability that the ion falling on the surface expels a sputtering product, and thus the computed yield is the true yield in the sense of the definition given in the first paragraph of this session regardless of the grain charge (i.e., n_ϕ/N_ϕ). To obtain the geometrical sputtering yield n_ϕ/N_0 at a given surface potential, the simulated sputtering yield should be multiplied by a factor of $(1 - e \cdot \phi/E_0)$, but we use the true yield, n_ϕ/N_ϕ, throughout this paper.

If we compare lines 1 and 2 in Table I, we can note about 50% increase in the measured sputtering yield for the sample bombarded simultaneously with 1-keV electrons, whereas the SRIM calculation predicts only 10%. An increase in the yield for the sample bombarded by a combination of electron and ion beams can also be seen in lines 3–5 of Table I. A number of sputtering sequences under given conditions in the third experiment was lower than that used in the previous experiments, and thus the error of the yield determination is higher. Nevertheless, this experiment undoubtedly confirms a decrease in the sputtering yield for samples charged to higher potentials that apparently contradicts to the results of Pavlů *et al.* [22]. They investigated the sputtering of gold spherical samples by energetic Ar ions without a compensation of the ion beam charge and found the yield enhanced by a factor of two with respect to the data expected for spherical samples. This effect was ascribed to a possible influence of the high electric field at the sample surface, and the authors suggested that such an enhancement would be even more pronounced for samples from insulators; however, we have found an opposite effect.

An increase in the sputtering yield observed in the case of simultaneous electron bombardment could be caused by the increase in the grain temperature because the electron beam delivers additional heat to the grain. The grain is levitating in the vacuum vessel ($\approx 10^{-8}$ mbar), and it is heated by the IR radiation form the vessel walls, by a laser beam used for a detection, and by ion and electron beams. The heat emitted by a 1-μm grain at 300 K is $\approx 1.5 \times 10^{-9}$ W, and the same power would receive the grain from the walls of the vessel. The laser beam heats the grain with $\approx 1.7 \times 10^{-11}$ W, the ion beam adds $\approx 7 \times 10^{-12}$ W, and the electron beam contributes up to $\approx 1.8 \times 10^{-11}$ W. It means that the total power added by a laser and particle beams represents only several percents of the power received from the vessel walls. A simple estimation using a black body approximation would lead to several degrees of the grain temperature increase. A more precise estimation of a heat balance under very similar conditions made in [34] led to the grain temperature increase by 30 K. It means that the observed increase in the yield when the positive grain charge is compensated for by the electron beam cannot be connected with the increase in the grain temperature.

Simultaneous applications of ion and electron beams would lead to a partial recombination of Ar ions. However, ion and electron beams are perpendicular in our experiment, and thus the interaction volume is about 1 mm^3 only. It means that the influence of neutral Ar atoms on the measured sputtering yield is negligible. The published values of the yield of SiO_2 sputtering by 2-keV Ar ions vary from 0.8 to 2 SiO_2/ion for a normal incidence angle (see [35] for a review). The yield averaged over a spherical sample would be enhanced by a factor of 1.2–2 due to its angular dependence [22], and thus our results fit into the published range of values.

Sputtering of oxides often exhibits preferential sputtering of oxygen by both electron [31] and ion [32] impacts in a

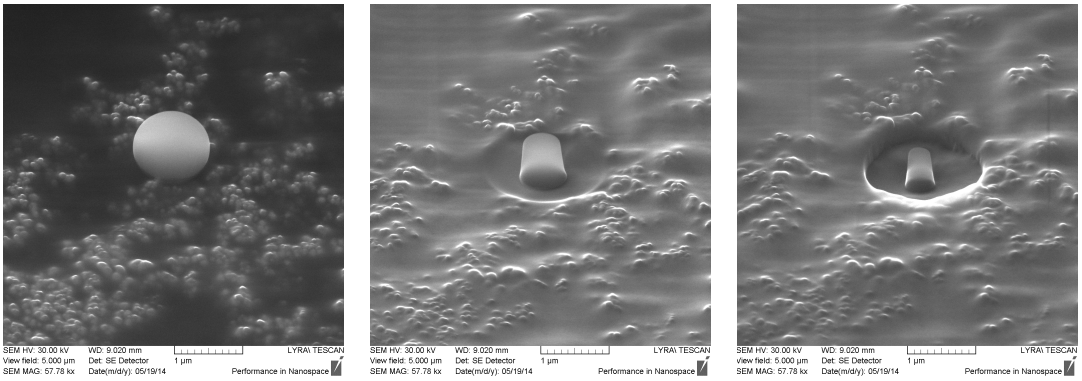

Fig. 3. SEM images of the glass grain sputtered by a 30-keV Ga^+ beam (293 pA, sputtered diameter 1.6 μm) (a) prior to sputtering and after (b) 4 and (c) 9 s.

comparison with the bombardment by neutral atoms. This effect was investigated because it could spoil the measurements of a surface composition by widely used Auger electron spectroscopy. Yakabe *et al.* [16] found that the electron bombardment increases the sputtering rate of SiO_2 by 1-keV Ar ions, and this increase is a linear function of the electron beam current density and it is roughly independent on the beam energy in the range of 1–5 keV. The authors reported an increase by a factor of two if the electron current density was as large as 150 A/m^2. Current densities in our experiment are several orders of magnitude lower ($\approx$2.5 mA/m^2), and thus this effect would be negligible. The other difference is that they irradiated the sample with ions and electrons sequentially, but both beams are simultaneously applied in our experiment. Unfortunately, Yakabe *et al.* [16] do not give the time delay between the electron and ion beam applications. Since a major effect of the electron beam would be connected with the modification of the crystalline structure of the surface, it is possible that the time delay between the electron and ion bombardments could be sufficient for a partial reconstruction of the surface. On the other hand, Yakabe *et al.* [16] investigated the sputtering of a planar thin SiO_2 film grown on the Si(100) substrate under normal incidence, whereas we sputtered small spherical samples. The difference in efficiency of the electron bombardment on an increase in the sputtering yield can be thus connected with the angular dependence of both processes; we will discuss this topic in the next section.

III. Sputtering of Grains Attached to a Surface

This experiment utilizes the scanning electron microscope (SEM) with the integrated focused ion beam system that uses an intense beam of 30-keV Ga ions for a very localized ($\approx$5-nm spot) sputtering. Since there is a possibility of the scanning of the ion beam over an area, we have used this facility for investigations of the angular dependence of the sputtering yield. The grain was fixed on a carbon tape, and the SEM image was stored. The ion beam was then scanned over the area larger than the grain for one or more seconds, and a new image was stored. Fig. 3 shows a series of images with a time span of about 5 s. By contrast to our previous experiments, the sputtering is rather fast because the grain decreases to about one-half of its mass within 5 s. Another interesting feature is a change in the grain shape from a sphere to a truncated cone.

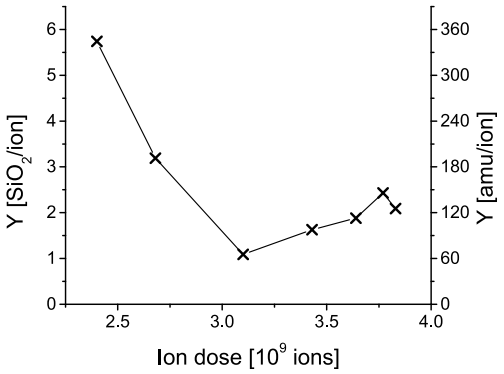

Fig. 4. Sputtering yield of the dust grain on the surface influenced by 30-keV Ga^+ ions as calculated from the size of the grain residual.

The sputtered mass was calculated from the estimated volume and used for the computation of the sputtering yield. Note that the images were taken from an angle of 50° from the ion beam axis and we expect rotational symmetry of the dust grain residuals. The determined yield, Y, as a function of the ion dose is presented in Fig. 4. Although the yield was independent on the ion dose in our previous experiments, it changes from about six to two in the first two steps and it remains about constant then. We suggest that this change of the integrated yield is connected with its angular dependence. The parts of the grain illuminated by the ion beam under an angle corresponding to the yield maximum are sputtered out within the first two steps, and the sputtering shapes the grain residual into a form with about constant sputtering rate along the surface.

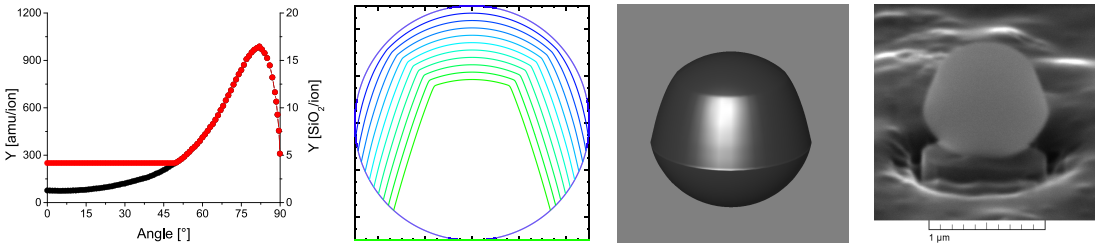

Fig. 5. (a) Angular profile of the sputtering yield from the TRIM software package (black dots) and our modification (red line). (b) Cross section of the grain illustrating a change of the grain shape as calculated by TRIM with our modification of the angular yield profile. (c) 3-D view of our simulation of the sputtering with the angular dependence corresponding to the red line in (a). (d) SEM image of the spherical grain after 60 s of the sputtering by a 30-keV Ga ion beam with current of 1 pA.

In order to check this suggestion, we developed an iterative routine for a description of the sputtering process under a changing shape of the sample that uses the TRIM software package for a computation of the sputtered volume. The black dots in Fig. 5(a) show the angular dependence of the sputtering yield from the TRIM code, and we used it in the first simulations. However, this angular profile did not explain the observed changes of the grain shape because the top part was sputtered too slowly. For this reason, we have increased the yield at low incidence angles to receive a better matching of the computation results with the experiment. The modification of the yield angular profile is shown by the red line in Fig. 5(a). Fig. 5(b) shows cross sections of the grain in several equidistant time steps, and we can note that modeled shapes correspond well to the photos in Fig. 3. A very good agreement of the computer model and experiment can also be inferred from a comparison of Fig. 5(c) and (d). Unfortunately, the errors in estimations of the sputtered volume from the images are relatively large, and thus we cannot say if the problem is in underestimation of the yield at low incidence angles rather than in overestimation of yields for large angles. Although the resulting shapes of grains after several sputtering sessions were qualitatively the same, a notable difference was observed. For example, the slopes of the cone in Fig. 3(b) and (c) are steeper than those in Fig. 5(d). We think that the difference is connected with a slightly different angular dependence of the sputtering yields for these two samples rather than with different intensities of the ion beam, but a nonlinear effect at very large beam intensities cannot be excluded. Nevertheless, this technique for a determination of the sputtering rate is completely new and we hope that we will be able to elaborate it to provide quantitative information as well.

IV. Conclusion

The experiments with levitating SiO_2 spherical grains sputtered by 2-kev Ar^+ ions provided an integrated sputtering yield of 1.0 SiO_2 molecules per incident ion. This yield increases to 1.6 when the grain is simultaneously bombarded by the intense 1-keV electron beam. The decreasing in the electron beam current density to a value comparable with the ion beam current density (2.5 mA/m^2) leads to intermediate value of the sputtering yield (1.3). The changes of the electron beam current density were accompanied with the changes of the electric field at the grain surface from 1.7×10^9 V/m for the pure ion sputtering to 16×10^7 V/m for the electron current densities exceeding the ion current. The observed changes of the sputtering yield cannot be caused by the changes of the surface electric field because their trend (decrease in the sputtering yield with an increasing surface electric field) is opposite to that found in [22]. We suggest that the observed effect can be caused by a modification of the grain surface by the electron beam that leads to the weakening of the bonding forces. This effect is probably strong enough to mask the dependence of the yield on the surface field. SiO_2 is a principal constituent of dust grains in the space, and these grains are bombarded by both ions and electrons simultaneously. The investigated effect thus can lead to a faster destruction of the small grains than expected. However, we cannot exclude that the increase in the sputtering yield by an electron impact depends on the electron energy (1 keV in our case).

The investigation of the sputtering of individual grains by a parallel beam has shown that it results in a change of the original spherical shape to the shape resembling a truncated cone. An attempt to model this process revealed that the TRIM software package probably underestimates the sputtering yield for small incident angles or overestimates it for large angles [Fig. 5(a)]. Note that this software is broadly used for the calculation of sputtering yields in industrial or scientific applications where the angular dependence of the yield can be important.

Acknowledgment

The authors would like to thank I. Matolínová for the help with scanning electron microscope–focused ion beam system measurements and Prof. D. Vítek for the useful and suggestive comments.

References

[1] R. E. Johnson, "Plasma-induced sputtering of an atmosphere," *Space Sci. Rev.*, vol. 69, nos. 3–4, pp. 215–253, 1994.
[2] T. J. Stubbs, R. R. Vondrak, and W. M. Farrell, "A dynamic fountain model for lunar dust," *Adv. Space Res.*, vol. 37, no. 1, pp. 59–66, 2006.
[3] A. L. Sprague, R. W. H. Kozlowski, D. M. Hunten, W. K. Wells, and F. A. Grosse, "The sodium and potassium atmosphere of the moon and its interaction with the surface," *Icarus*, vol. 96, no. 1, pp. 27–42, 1992.
[4] P. Wurz *et al.*, "The lunar exosphere: The sputtering contribution," *Icarus*, vol. 191, no. 2, pp. 486–496, 2007.

[5] L. V. Starukhina, "Computer simulation of sputtering of lunar regolith by solar wind protons: Contribution to change of surface composition and to hydrogen flux at the lunar poles," *Solar Syst. Res.*, vol. 37, no. 1, pp. 36–50, 2003.
[6] T. Järvi and K. Nordlund, "Sputtering of freestanding metal nanocrystals," *Nucl. Instrum. Methods Phys. Res. B, Beam Interact. Mater. Atoms*, vol. 272, pp. 66–69, Feb. 2012.
[7] H. M. Urbassek, R. M. Bradley, M. L. Nietiadi, and W. Möller, "Sputter yield of curved surfaces," *Phys. Rev. B*, vol. 91, no. 16, p. 165418, 2015.
[8] T. A. Cassidy and R. E. Johnson, "Monte Carlo model of sputtering and other ejection processes within a regolith," *Icarus*, vol. 176, no. 2, pp. 499–507, 2005.
[9] B. Hapke and W. Cassidy, "Is the Moon really as smooth as a billiard ball? Remarks concerning recent models of sputter-fractionation on the lunar surface," *Geophys. Res. Lett.*, vol. 5, no. 4, pp. 297–300, 1978.
[10] R. Cheng, T. Wang, Y. Zhao, Y. Wang, H. Peng, and G. Xiao, "Potential sputtering on SiO_2 and Au induced by highly charged ions impact," *J. Phys. Conf. Ser.*, vol. 488, no. 13, p. 132039, 2014.
[11] A. F. Barghouty, F. W. Meyer, P. R. Harris, and J. H. Adams, Jr., "Solar-wind protons and heavy ions sputtering of lunar surface materials," *Nucl. Instrum. Methods Phys. Res. B, Beam Interact. Mater. Atoms*, vol. 269, no. 11, pp. 1310–1315, 2011.
[12] F. Aumayr and H. Winter, "Potential sputtering," *Philos. Trans. Roy. Soc. A-Math. Phys. Eng. Sci.*, vol. 362, no. 1814, pp. 77–102, 2004.
[13] F. W. Meyer, P. R. Harris, C. N. Taylor, H. M. Meyer, III, A. F. Barghouty, and J. H. Adams, "Sputtering of lunar regolith simulant by protons and singly and multicharged Ar ions at solar wind energies," *Nucl. Instrum. Methods Phys. Res. B, Beam Interact. Mater. Atoms*, vol. 269, no. 11, pp. 1316–1320, 2011.
[14] A. Kracher, F. Aumayr, D. W. G. Sears, and M. Kareev, "Space weathering by highly charged heavy ions in the solar wind," *Meteoritics Planetary Sci.*, vol. 38, p. 5204, Jul. 2003.
[15] H. Hijazi *et al.*, "Anorthite sputtering by H^+ and Ar^{q+} ($q = 1$–9) at solar wind velocities," *J. Geophys. Res.*, vol. 119, no. 10, pp. 8006–8016, 2014.
[16] T. Yakabe, D. Fujita, and K. Yoshihara, "Electron irradiation effect on depth profiling of a SiO_2/Si(1 0 0) surface by Auger electron spectroscopy," *Appl. Surf. Sci.*, vol. 241, nos. 1–2, pp. 127–130, 2005.
[17] W. Eckstein, "Sputtering yields," in *Sputtering by Particle Bombardment* (Topics in Applied Physics), vol. 110. Berlin, Germany: Springer, 2007, pp. 33–187.
[18] S. Zimmermann and H. M. Urbassek, "Sputtering of nanoparticles: Molecular dynamics study of Au impact on 20 nm sized Au nanoparticles," *Int. J. Mass Spectrometry*, vol. 272, no. 1, pp. 91–97, 2008.
[19] J. P. Biersack and W. Eckstein, "Sputtering studies with the Monte Carlo program TRIM.SP," *Appl. Phys. A*, vol. 34, no. 2, pp. 73–94, 1984.
[20] J. F. Ziegler, "SRIM-2003," *Nucl. Instrum. Methods Phys. Res. B, Beam Interact. Mater. Atoms*, vols. 219–220, pp. 1027–1036, Jun. 2004.
[21] M. L. Nietiadi, L. Sandoval, H. M. Urbassek, and W. Möller, "Sputtering of Si nanospheres," *Phys. Rev. B*, vol. 90, no. 4, p. 045417, 2014.
[22] J. Pavlů, I. Richterová, Z. Němeček, J. Šafránková, and J. Wild, "The sputtering of dust grains: Aspects of experimental observations," *IEEE Trans. Plasma Sci.*, vol. 35, no. 2, pp. 297–302, Apr. 2007.
[23] J. Pavlů, "Mass-loss rate for MF resin microspheres," *IEEE Trans. Plasma Sci.*, vol. 32, no. 2, pp. 704–708, Apr. 2004.
[24] J. Pavlů, I. Richterová, Z. Němeček, J. Šafránková, and I. Čermák, "Interaction between single dust grains and ions or electrons: Laboratory measurements and their consequences for the dust dynamics," *Faraday Discussions*, vol. 137, pp. 139–155, Jul. 2008.
[25] Z. Němeček *et al.*, "Lunar dust grain charging by electron impact: Dependence of the surface potential on the grain size," *Astrophys. J.*, vol. 738, no. 1, p. 14, 2011.
[26] J. Goree, "Charging of particles in a plasma," *Plasma Sour. Sci. Technol.*, vol. 3, no. 3, pp. 400–406, 1994.
[27] V. E. Fortov, A. V. Ivlev, S. A. Khrapak, A. G. Khrapak, and G. E. Morfill, "Complex (dusty) plasmas: Current status, open issues, perspectives," *Phys. Rep.*, vol. 421, pp. 1–103, Dec. 2005.
[28] R. Behrisch and W. Eckstein, *Sputtering by Particle Bombardment* (Topics in Applied Physics), vol. 110. Berlin, Germany: Springer, 2007.
[29] D. Urrabazo, J.-F. Veyan, M. J. Goeckner, and L. J. Overzet, "Ion induced electron emission from chemically cleaned Si and Ge," *J. Phys. D, Appl. Phys.*, vol. 48, p. 405201, Oct. 2015.
[30] M. Vyšinka, J. Vaverka, J. Pavlů, Z. Němeček, and J. Šafránková, "Sputtering of glass dust grain by ions and electrons," in *WDS Proceedings of Contributed Papers—Physics*, J. Šafránková and J. Pavlů, Eds. Prague, Czech Republic: Matfyzpress, 2014, pp. 371–377.
[31] D. Fujita, K. Onishi, T. Yakabe, and K. Yoshihara, "Electron beam effects on AES depth profiling of SiO_2 thin film on Si(001): A factor analysis study," *J. Surf. Anal.*, vol. 13, no. 2, pp. 190–199, 2006.
[32] T. Mizutani, "Preferential sputtering of oxygen from SiO_2 by low-energy ion beam and neutral beam bombardment," *Jpn. J. Appl. Phys.*, vol. 30, no. 4A, pp. L628–L631, 1991.
[33] J. Pavlů, I. Richterová, Z. Němeček, and J. Šafránková, "Field emission characteristics of gold dust grains," *Adv. Space Res.*, vol. 42, no. 1, pp. 129–135, 2008.
[34] M. Beránek, M. Vyšinka, J. Pavlů, I. Richterová, Z. Němeček, and J. Šafránková, "Dust as a gas carrier," *IEEE Trans. Plasma Sci.*, vol. 38, no. 4, pp. 886–891, Apr. 2010.
[35] M. P. Seah and T. S. Nunney, "Sputtering yields of compounds using argon ions," *J. Phys. D, Appl. Phys.*, vol. 43, no. 25, p. 253001, 2010.

Marek Vyšinka was born in Brno, Czech Republic, in 1984. He received the M.S. degree from Charles University in Prague, Prague, Czech Republic, in 2008, where he is currently pursuing the Ph.D. degree with the Department of Surface and Plasma Science, Faculty of Mathematics and Physics.

His current research interests include laboratory simulation of elementary processes in dusty plasmas.

Zdeněk Němeček was born in Prague, Czech Republic, in 1947. He received the M.S., Ph.D., and D.Sc. degrees from Charles University in Prague, Prague, in 1971, 1982, and 1996, respectively.

He has held several leading positions with the Faculty of Mathematics and Physics, Charles University in Prague, since 1971. His current research interests include solar wind interaction with the Earth's magnetosphere and the laboratory simulations of plasma processes.

Jana Šafránková was born in Teplice, Czech Republic, in 1947. She received the M.S., Ph.D., and D.Sc. degrees from Charles University in Prague, Prague, Czech Republic, in 1972, 1982, and 1996, respectively.

She has held several positions with the Faculty of Mathematics and Physics, where she is currently the Head of the Space Physics Laboratory. Her current research interests include solar wind and laboratory simulations of elementary processes in dusty plasmas.

Jiří Pavlů was born in Pardubice, Czech Republic, in 1977. He received the M.S. and Ph.D. degrees from Charles University in Prague, Prague, Czech Republic, in 2001 and 2005, respectively.

He is currently a Senior Assistant with the Space Physics Laboratory, Department of Surface and Plasma Science, Faculty of Mathematics and Physics, Charles University in Prague. His current research interests include laboratory investigations of elementary processes on dust grains induced by electron, ion, and photon irradiations.

Jakub Vaverka was born in Prague, Czech Republic, in 1983. He received the M.S. and Ph.D. degrees from Charles University in Prague, Prague, in 2008 and 2015.

He is currently at Postdoctoral research position with the Umeå University, Sweden. His current research interests include study of dust impact plasma generated on CLUSTER spacecraft and detected by its antennas.

Jaroslava Lavková was born in Poprad, Slovakia, in 1988. She received the M.S. degree from Charles University in Prague, Prague, Czech Republic, in 2012, where she is currently pursuing Ph.D. degrees under the cotutelle program in cooperation with the University of Burgundy, Dijon, France.

Her current research interests include surface and interface physics is focused on thin layers systems studied by techniques of electron microscopy (scanning and transmission electron microscopes, focused ion beam) and electron spectroscopy.

Příloha A4.

Vyšinka, *M.*, Nouzák, *L.*, Pavlů, *J.*, Němeček, *Z.*, Šafránková, *J.*, *a* Richterová, *I. MF Microspheres: Helping or Puzzling Tool? odesláno do* IEEE Trans. Plasma Sci., *2017*

MF Microspheres: Helping or Puzzling Tool?

Marek Vyšinka, Libor Nouzák, Jiří Pavlů, Zdeněk Němeček, Jana Šafránková, Ivana Richterová

***Abstract*—Melamine formaldehyde (MF) microspheres are widely used in dusty plasma experiments for their monodispersity, sphericity, low mass density, and well defined sizes. The paper summarizes problems that were encountered in numerous applications of these grains in different laboratory simulations. and the already published results are discussed in view of new experiments. The main results of this paper are connected with changes of the grain mass due to the decreased pressure and/or increased temperature and variations of the grain dimensions, its shape, and mass density under electron or ion bombardments. By contrast to the work function estimated from field emission properties, we have found the photoelectric work function (4.5 eV) being close to that expected. A sputtering of the grains using a 30 keV ion beam revealed their unexpected heterogeneity.**

***Index Terms*—Dust grains, dusty plasma, melamine formaldehyde (MF) resin, microspheres.**

I. Introduction

MELAMINE formaldehyde resin spheres are widely used by the dusty plasma community since they are available in a broad range of sizes and their low-mass density and a good optical reflectivity (see Table I adopted from Microparticles GmbH web pages http://microparticles.de/en/) facilitate different experimental techniques. Monodispersity and sphericity make estimations and calculations easier; the low-mass density enables easy grain levitation and the high reflectivity implicates easy optical detection. From this point of view, it seems that MF microspheres are an ideal sample not only for the dusty plasma research, but for many sorts of studies involving small particles; even more, they are offered in numerous alternatives with functional surfaces (dyed, metal covered, fluorescent, with magnetic layer, etc.).

Numerous dusty plasma experiments over the world used MF grains: their different sizes were used together onboard ISS within the PKE-Nefedov, PK-3 Plus, and PK-4 experiments, e.g., [1]–[3]; they were used as a kind of probes in order to study and to map electric fields (both horizontal and vertical) [4], [5] in low-pressure gas discharges; or to investigation of interactions between the plasma and magnetic field [6]; to study dust grains under the influence of crossed electric and magnetic fields in the sheath of an RF discharge [7]; or dust charge fluctuations in the sheath and at its boundaries [8], [9]; to determination of levitation limits within the sheath [10]; and to demonstration of vortex flow turbulence [11] in complex plasma experiments. Liu et al. [12] reported how the radiation pressure and gas drag forces act on a single MF microsphere and quantified the Epstein gas drag force coefficient. In space applications, Wang et al. [13] discussed a dust transport in the plasma investigating an origin of the lunar horizon glow.

TABLE I
SOME OF THE PROPERTIES OF MF PARTICLES (ADOPTED FROM THE PRODUCER WEB PAGES).

Property	MF particles
Density	1.51 g/cm^3
Refractive index	1.68
Particle diameter	0.3–12 μm
Monodispersity	CV $< 5\%$
Particle shape	spherical
Temperature stability	to 250 °C
Mechanical strength	robust
Stability in solvents without swelling	water, alcohols, all solvents and oils
Structure	hydrophilic, non-porous

Above a brief overview of the literature demonstrates how popular the MF grains are in fundamental laboratory studies. Nevertheless, many authors have found that some parameters of MF grains change during experiments and that these variations depend on types of the plasma environment and on applications of various diagnostic techniques (e.g., [14]–[16]). According to these papers, we already know that an exposition of MF grains to vacuum, plasma, and/or electron or ion beams can induce changes of the MF grain dimensions, mass density, shape, and electrical properties that can be attributed to the modification of the internal structure. Since this knowledge is spread over different reports, we summarize and comment the previous results and show the results of new observations with a motivation to help other experimenters to understand and to interpret their measurements.

The text is divided into the subsections devoted to different aspects of MF grains (work function, mass, size, mass density, adhesiveness of surface layers, etc.) or processes like field emission or ion sputtering. Each of these subsections starts with a short overview of already published experiments that are further discussed from the point of view of properties of MF grains, and continues with new results. The main attention is focused on an interaction of MF particles with energetic electrons or ions using two types of experiments but other possible sources of particle modifications are discussed as well.

II. Experimental techniques

The paper presents two complementary types of experiments. Scanning Electron Microscopy (SEM) is a widely used

This work was supported by the Czech Science Foundation project 16-05762S and LN thanks to the Grant Agency of Charles University for support by project 728616.

All authors are with the Charles University in Prague, Faculty of Mathematics and Physics, Prague, Czech Republic. e-mail: (see http://physics.mff.cuni.cz/kfpp/).

technique for scientific images under an assumption that the energetic electrons do not change the properties of investigated samples substantially. For this reason, we have varied the focus, scanned area, and electron beam intensity in course of the experiments. High intensities and long expositions were used to influence the grains, whereas very low intensities served for consecutive images that permit a quantification of results of the electron beam–grain interaction. The electron beam energy was 15 keV and the pressure in the experimental vessel varied from 10^{-2} to 10^{-3} Pa during experiments. The integrated-in Focused Ion Beam (FIB) operating with 30 keV gallium ions facilitated sputtering experiments.

A second type of our experimental set-ups is an electrodynamic quadrupole trap [17] which allows us to catch a single charged grain and to affect it by different beams of particles with a tunable energy. This particular experiment is conducted under ultra-high vacuum conditions (typically 10^{-7} Pa). The principles of this technique can be found in [14] and in [18], respectively, thus we repeat only basic features used in the present paper.

A single charged MF grain levitates in the effective potential of the trap and it can be bombarded by beams of UV photons and/or beams of electrons and/or ions. The only measurable quantity is a frequency of grain oscillations that is directly proportional to its charge-to-mass ratio (specific charge hereafter). A determination of all important quantities requires applications of dedicated techniques:

1) Grain mass: the charge of a slightly charged (about one hundred of elementary charges) grain is changed by one elementary charge up or down and a jump of the oscillation frequency is proportional to the grain mass.
2) Grain charge: it is computed from the specific charge and grain mass.
3) The surface potential: the grain is charged by the ion beam to a positive surface potential (that is approximately equal to the beam energy) and the beam energy is abruptly decreased. The beam ions are repulsed from the charged grain but it is gradually discharged by background electrons (originated mainly due to ionization of the residual gas in the vessel). When the grain potential becomes equal to the beam energy, an abrupt change of the discharging current is observed.
4) Grain specific capacitance: it can be calculated from its specific charge corresponding to the potential determined by the point 3).
5) Grain size: it is calculated from the capacitance under an assumption of the grain spherical shape.

If the mass determined by 1) and the estimated size by 5) do not match the known mass density, it can be interpreted as a non-spherical shape of the grain or mass density change.

III. Observations

A. Work function

As a first point, we discuss the work function that is a very important parameter for any estimation of the charge of illuminated dust grains, nevertheless, its determination is generally difficult for insulators due to their charging. For this reason,

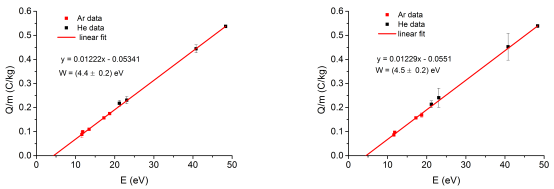

(a) (b)

Fig. 1. Work functions of the MF grain calculated from identified emission lines of Ar I, Ar II, He I and He II prior to (left) and after (right) 35-hour treatment by the 0.4 keV electron beam.

Pavlu et al. [19] tried to estimate the work function of MF grains from observations of the field emission discharging of highly charged grains by the Fowler–Nordheim method. Since the resulting plots were neither linear nor stable, the authors were able to provide only a very broad range (1.4–7.5 eV) of work function values. Suggested causes of the spread of experimental data were variations of the electric capacitance caused by unpredictable changes of the grain dimensions or shapes due to a high surface electric field. It was one of the first experiments showing that the geometry/dimension of MF grains can be significantly influenced by their charge.

As a range of MF work functions established by [19] was rather broad, we applied the method based on the photoemission that was suggested by [20]. Impacts of UV photons lead to charging of the MF grain by photoelectron emission. The grain surface potential is given by the photon energy and the material work function according to Eq. 1.

$$\phi = \frac{1}{e}(h\nu - W) \tag{1}$$

where ϕ is the surface potential, h is the Planck constant, ν is the photon frequency, W is the work function and e is the elementary charge. A determination of the work function would be straightforward if a single UV line would be used. However, above mentioned problems with the surface electric field require the measurements with several photon energies. We used the UV lamp that mixes wavelengths according to discharge conditions and the work function was extrapolated from the measurements at the emission lines of argon (11.62 eV, 11.83 eV, 13.47 eV, 17.26 eV, and 18.72 eV) and helium (21.22 eV, 23.08 eV, 40.82 eV and 48.35 eV).

The extrapolated work function of the grain was W=(4.4 $\pm$ 0.2) eV (Fig. 1, left). To check a possible influence of the electron bombardment on the work function, the grain was bombarded for 35 hours by the 0.4 keV electron beam and the work function was determined again (Fig. 1, right). The observed change of the work function (4.5 ± 0.2) eV is within the estimated error of measurements. Moreover, the oscillations of the grain in the trap were stable and it suggests that a specific capacitance of the grain did not change in course of the experiments.

B. Mass and mass density changes in vacuum

A MF resin is known to be hydrophilic and the grains tend to absorb water from the air during their storage. In dry

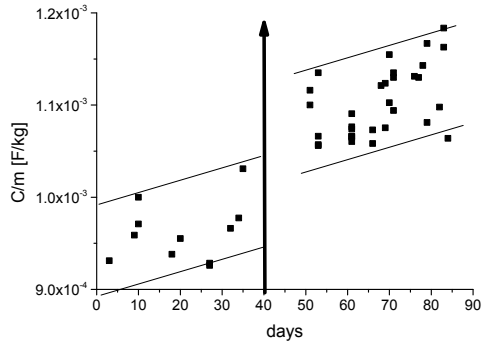

Fig. 2. An evolution of the specific capacitance of 10-micron MF grains in UHV conditions. The arrow marks the time of the grain baking at $240\,^{\circ}$C for 6 hours.

environments or at lower pressures, an evaporation of water or other volatile elements would lead to mass changes [15]. However, it is not clear whether these changes result in a decrease of the mass density and the dimensions are constant during the time or not. To clarify this point, we have revisited first systematic measurements of a evolution of the MF grain mass in UHV conditions by [14]. The authors carried out two particular experiments:

- Measurements of the mass loss rate of one weakly charged MF grain with diameter of $2.4\,\mu$m that was kept in UHV conditions (with the pressure of 10^{-6} Pa) and the specific charge was recorded for 6 days. Since an overall change of the specific charge was lower than that corresponding to one elementary charge, the whole change should be caused by the decrease of the particle mass.
- Measurements of a evolution of the specific capacitance of larger ($10\,\mu$m) grains for 40 days that were followed by 6 hours of baking at $240\,^{\circ}$C and by new measurements of the specific capacitance for next 45 days (see Fig. 2). During the observations, they used an assemblage of about 50 particles; each of them was measured only once to minimize the effects of bombardment with energetic electrons or ions. We cannot exclude an influence of these measurements on the grain parameters but this effect would be the same for each measured grain, thus the obtained trends are reliable.

Results of these two experiments can be summarized as:

(a) A monotonic increase of the specific charge with a rate of 0.011% a day that corresponds to the decrease of the mass of the grain with diameter of 2.4 μm with a rate of 1.2×10^{-18} kg/day (i.e., 0.015% a day).

(b) A monotonic increase of the specific capacitance of the 10 μm grain with a rate of about 0.09% a day during an exposition to UHV and the additional 6.3% increase during baking. The data are shown in Fig. 2 as squares, the thin straight lines show the average trend derived in two halves of the plot (prior to and after the baking), and their distance corresponds to an uncertainty of the grain diameter declared by the manufacturer. Note that Fig. 5 in [14] shows a reciprocal value of the specific capacitance in arbitrary units, thus the plot exhibits a decreasing trend of the depicted quantity, nevertheless, the initial data are the same.

The interpretation of results in terms of the mass density, volume, etc. requires additional assumptions and their application can lead to different results:

1) Assumptions of an unaffected grain diameter and measurements in (a) result in a decrease of the mass density with a rate of 0.011% a day. On the other hand, the assumption of a constant diameter (constant capacitance) and measurements in (b) provide a decrease of the mass density with a rate of 0.09% a day. An order of magnitude difference cannot be probably explained by different grain diameters used for measurements (2.4 and 10 μm, respectively) that could result in a different relative mass loss rate, thus this assumption should be abandoned.
2) The specific capacitance is inversely proportional to a product of the mass density and a square of the grain diameter. Measurements in (b) show an overall relative increase of the specific capacitance of about 8% (the effect of baking is not considered) and the assumption of the constant mass density thus requires a decrease of the grain diameter by 4%. Such a decrease is smaller than that reported by [16] in the discharge plasma but our assumption of the constant mass density would lead to the mass decrease to 88% of the original value that is probably too large if the mass loss rate determined in the measurements (a) is considered.
3) The principal assumption that the grains conserve their spherical shape is behind both scenarios discussed above. It seems to be very natural expectation but, in a light of phenomena that will be described in the further text, we should stress it out. For the sake of completeness, we are showing how the specific capacitance depends on the grain shape in Fig. 3. The plot depicts a ratio of capacitances of ellipsoid of revolution and sphere with the same volume. One can see that this ratio is always larger than unity. It means that the change of the grain shape could contribute to the observed increase of the specific capacitance.
4) Since our above considerations did not lead to a satisfactory conclusion, we suggest that the results of the experiment should be interpreted as simultaneous changes of the mass density and a volume of the grain. However, the data provided by the mentioned experiments are not sufficient for determination of a proportion of changes of these two parameters.

Nevertheless, the experiments undoubtedly confirmed a fact that MF grains loss their mass in the vacuum even if they are not affected by electron or ion bombardments, and allowed to determine the mass loss rate. The mass losses are accompanied with a decrease of grain dimensions and changes of the mass density. It would be interesting to know if the mass losses are

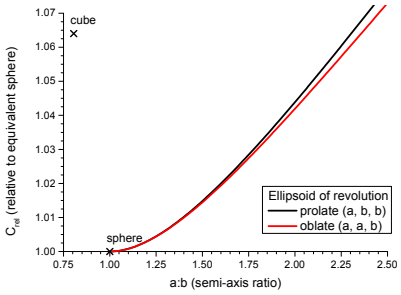

Fig. 3. A ratio of capacitances of the ellipsoid of revolution and sphere with the same volume as a function of the aspect ratio.

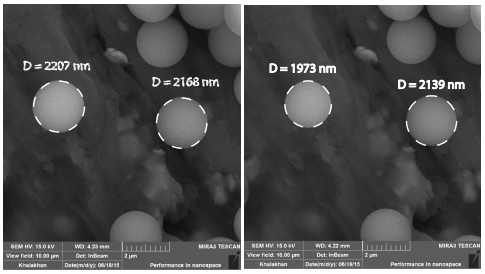

Fig. 4. Influence of the electron bombardment (the beam of 15 keV, with the intensity of 71 A/m^2) on the MF grain size. (a) prior to bombardment, (b) after 40-minute bombardment (the grain on the left side of both images was bombarded, the grain on the right side serves to a comparison).

proportional to the grain mass or to the grain surface but the experimental data are not sufficient to answer this question.

C. Evolution of the grain size under electron bombardment

The grains immersed in a plasma are bombarded by plasma particles. In a majority of applications, the plasma is non-isothermal and electrons are much hotter than the ions or neutral atoms that often follow the room temperature. Consequently, the energies of impinging electrons are larger and thus one would expect that the effects of a grain bombardment (if any) would be caused by electrons. [21], [22] studied an oxygen plasma etching and a layer deposition on the MF grain surface. They observed a grain size linearly decreasing with the time (in first 23 minutes, 8% reduction of a grain diameter was recorded). Since most experiments on dusty plasmas use argon, chemical etching is often neglected. Nevertheless, [16] observed the 6% size reduction during baking at 120 °C that is consistent with the results of [14] and about the 18% size reduction during applications of 4 h of operation of the RF discharge in argon [16]. Size changes were observed via evolving Mie scattering signal and also *ex situ* by the microscopy. These rates are much larger than those determined in UHV conditions and thus their enhancement would be probably attributed to the electron bombardment.

[23] studied the secondary electron emission from MF grains bombarded by high-energy electrons (5–10 keV) and observed a sudden change of the surface potential of the grain. Taken into account charging currents, the authors concluded that such instantaneous change cannot be caused by an increase of the grain charge and attributed it to a decrease of the grain effective radius due to a collapse. They speculated that the observed strange behavior can be caused by a grain deformation (changing shape and/or size) due to the inner electric field, resulting in a change of the electric capacitance. They observed up to about the 25% increase of the measured charge (Fig. 1, right in [23]), i.e., the capacitance (and thus a radius) should decrease by the same percentage if the surface potential and particle mass are expected to remain constant. These assumptions are well justified because the surface potential is given by a balance between incoming and outgoing electrons and ions that would not depend on the grain size or shape and the mass could not increase in the UHV conditions.

The size of small grains is usually exactly measured by electron microscope (EM) techniques. For example, Liu [12] reported transmission EM observations showing that the MF grains are smaller than specified by the manufacturer. However, the grains are bombarded by energetic electrons during EM measurements, and thus the results of such measurements should be taken with a care because the electron bombardment can change the grain diameter as we discussed above.

We have performed a series of SEM measurements in order to clarify an influence of energetic electrons on MF grain dimensions. Since the grain obtains a dose of electrons during measurements of its diameter, we have used two grains to separate effects caused by imaging from those resulting from an electron intensive bombardment. Fig. 4a shows these grains prior to the intensive electron bombardment. Their diameters are D_1 = 2207 nm and D_2 = 2168 nm, respectively, but the diameter would be 2350 nm ($\pm$ 40 nm) according to the manufacturer. The difference between measured and declared diameters cannot be caused by a decrease of the grain size in the vacuum mentioned above because the image was taken within first 20 minutes but we cannot exclude the influence of the electron beam.

After taking this image, the grain on the left-hand side was bombarded by the high-intensity 15-keV electron beam (its average current density was $\approx$ 71 A/m^2), the grain on the right-hand side was left unaffected for a comparison. Both grains obtained some electron dose during the SEM imaging but this dose was the same for both grains. SEM images were taken every 5 minutes of the electron bombardment. During 40 minutes of these operations, the left grain shrinks from 2207 nm to 1973 nm (11%), whereas the right grain shrinks from 2168 nm to 2139 nm (1.4%) only. The final image is shown in Fig. 4b.

Fig. 5 illustrates that the shrinking was approximately saturated after 30 minutes of the electron bombardment. Although the exact mechanism is unknown, it is evident that the electron bombardment affects the grain size. The black crosses show the results of measurements described above, other symbols stand for analogous measurements carried on different grains attached to Al and carbon substrates. The profiles in Fig. 5 confirm a decrease of the grain size under electron bombardments but the reduction rates are different.

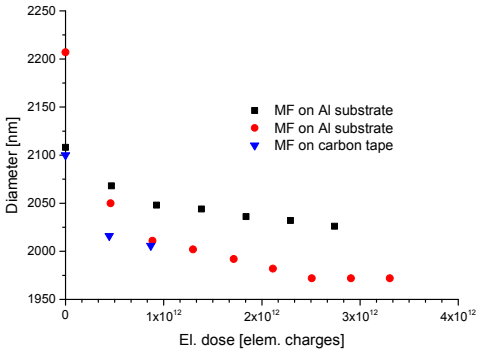

Fig. 5. A change of the MF grain diameter as a function of the electron dose (each data point was obtained after 5 minutes of the 15 keV electron bombardment). Two grains (red and black) were lying on the Al substrate and one grain (blue triangles) was attached to the carbon tape.

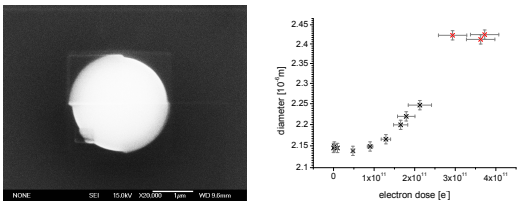

(a) (b)

Fig. 6. The MF grain bombarded by 15 keV electrons. (a) SEM image — upper left quarter of the grain was bombarded by electrons, upper right quarter is intact; (b) A diameter of the MF grain as a function of the electron dose (adopted from [24]).

In order to demonstrate a complex character of the interaction of MF grains with the electron beam, Fig. 6 shows the results of Pavlu et al. [24]. This experiment used another SEM facility allowing much higher beam intensities. The black points in Fig. 6b were obtained in a similar regime as the points in Fig. 5. We can see a small initial decrease of the grain diameter. The decreasing trend is consistent with Fig. 5 but this decrease is followed by a rapid increase for higher electron doses. Since this result was surprising, the authors have scanned only left upper quarter of the grain as it is shown in Fig. 6a and the corresponding red crosses in Fig. 6b belong to these scans. It can be seen that the increase of the grain size is strictly localized to the part that was affected by the electron beam.

D. Surface coating and its thickness

MF grains are offered in metal-coated versions (Au, Ni, Cu, Pt, ...) that would combine advantages of the low mass and metal surface. Two major problems concerning the metal layer were identified: (1) it is easily peeled off by energetic electrons (it can be caused by shrinking of the MF grain inside the metal crust as Fig. 7 illustrates using grains covered by the AU layer), and (2) the layer thickness does not meet expected values as it was shown by [25]. The authors adapted the secondary electron emission model to allow computations of the secondary emission from layered grains. They used MF spheres covered by a nickel layer as an example and a comparison with measured profiles of the secondary emission yield revealed that (unlike producer's expectations of the 100–200 nm thickness [26]), the thickness of the real Ni coating cannot exceed 20 nm. This result of computer simulations was confirmed by precise measurements of the mass distribution [25].

The experiments with Ni coated grains in SEM revealed another interesting peculiarity. Fig. 8 shows the grain fixed to a carbon tape prior to and after the bombardment by the 15-keV electron beam. The grain in the left panel obtained only a minimum dose of electrons needed for a creation of its image. The image demonstrates that the surface layer is not smooth and it is even not continuous. It is in an agreement with a small layer thickness discussed above. The middle panel presents a top view of the same grain after 30 minutes of the following electron bombardment. The grain radius is marked within the panel but one can note about a 50% particle increase even without such a tool. However, the grain is not only larger but its surface is very smooth. Moreover, the grain enlargement is not a simple inflation but it is connected with the change of the grain shape as a side view in the right panel shows.

An analysis of this and many other photos suggests that the grain is covered by a thick layer of a another material. To confirm this hypothesis, we used the FIB facility and cut the grain in half. The SEM photo of this cut is depicted in Fig. 9. Although the contrast of this image is not excellent, the important features can be identified. The dark core presents the MF grain with nearly unaffected size (in the horizontal direction) of $L1 = 2165$ nm. Its size in the vertical direction is probably smaller, $L1 = 1869$ nm. The grain core is bounded by a light thin layer of the original Ni coat; nevertheless, this coat seems to be removed at the top part of the grain. The whole grain is covered with a thick layer of unknown material but its outer boundary is rather diffusive in this photo.

A grow of a such layer was observed repeatedly for Ni covered MF grains attached to the carbon tape but we did not find this effect either for pure MF grains on carbon tape or for Ni covered grains fixed to an Al surface. Our interpretation of this observation is that the electron beam releases carbon atoms from the surface of the carbon tape and (probably) a volatile component of the MF resin. The catalytic properties of the Ni coat thus lead to synthesis of a new material that builds the layer on the grain surface.

E. Sputtering

Impacts of energetic ions lead to sputtering of a dust grain material. It is well known that the sputtering yield depends on the energy and mass of the ions and the direction of the ion velocity with respect to surface. Angular dependence of the sputtering yield leads to a modification of the shape of the originally spherical grain attached to a surface [27]. Also the surface morphology can change under the ion bombardment and surface ripples can be formed (e.g., [28], [29]).

We used 30 keV Ga ions from the focused ion beam (FIB) integrated into SEM to sputter MF grains. A sequence of photos of one grain sputtered with the beam intensity of

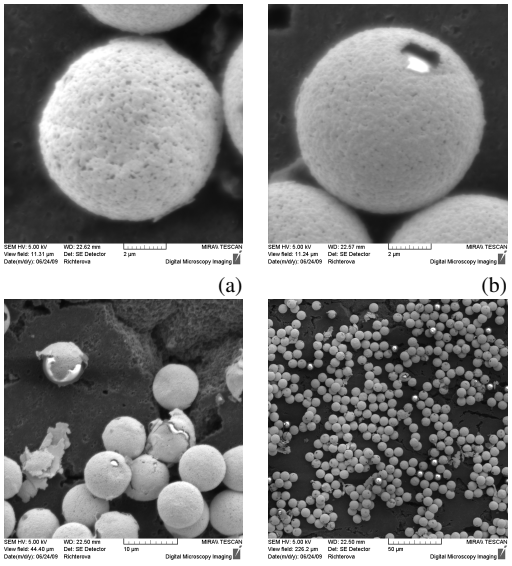

Fig. 7. SEM images of Au-coated MF grains: (a) a grain prior to the bombardment; (b) a detail of one grain after bombardment by 15-keV electrons (note that the Au layer is detached from the grain); (c) a destruction of the surface layer (it is rather common); and (d) a portion of grains is completely peeled off due to the electron bombardment.

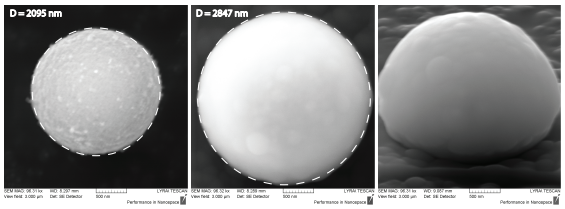

Fig. 8. An evolution of the grain size and shape during the bombardment by the 15-keV electron beam. The used sample: MF grain covered by Ni and fixed to a carbon tape for SEM diagnostics.

1 A/m^2 is shown in Fig. 10. A change of the grain overall shape seen in Fig. 10e is consistent with observations made on glass grains by Vysinka [27] and can be attributed to the angular dependence of the sputtering yield. However, this way of sputtering is not typical as Fig. 10f demonstrates. Moreover, the surface of the grain becomes rough with many shallow depressions even in early stages of sputtering (Fig. 10c).

Larger beam intensities amplify this effect as we show in Fig. 11 that presents the 2.4 μm MF grain prior to (a) and after (b) ion sputtering. The grain material is expected to be homogenous but holes through the grain are milled at some points. A creation of holes is probably connected with a strong angular dependence of the sputtering yield that can be inferred from the slope of the flanks of the sputtered particle in Fig. 11b. This effect seems to be more pronounced at larger intensities of the ion beam but we did not observe such behavior on other materials like SiO_2 (Fig. 11c) and glassy carbon (Fig. 11d).

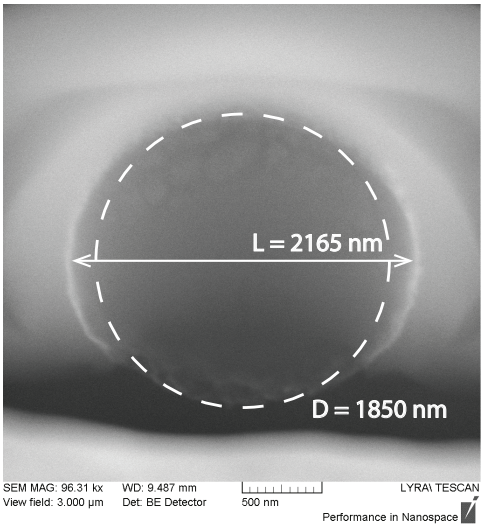

Fig. 9. The MF grain covered by Ni and fixed to a carbon tape after cutting in half by FIB. See the text for the detail explanation.

IV. Discussion

Despite many believes, the MF microspheres are not so stable as it is thought. They decrease their mass and diameter in UHV conditions, at raised temperatures, and under the influence of the electron beam with a very low intensity and energy, probably due to heating and evaporation of some water or other volatile components contained in the grain. The losses of the mass are as large as 1.2×10^{-18} kg/day for 2.4-micrometer grains. The spherical shape of the grain is probably not affected by these agents. On the other hand, larger energies of beam electrons result to notable, and sometimes abrupt changes of the grain dimensions. Its bombardment by energetic electrons usually leads to high surface potentials and it is not clear, whether the main cause of dimension changes is a destruction of the internal structure of the grains or the large electric field at the surface. We think that the small doses of electrons are probably sufficient to destroy the internal molecular structure and it results to the initial decrease of the grain diameter, whereas the large electric field causes a consecutive inflation of the grain.

However, in a view of new experiments (Figs. 8 and 9), we cannot exclude another interpretation of the observed grain growth that is related to the SEM experiments. The pressure in SEM facilities is usually rather moderate and a residual gas can contain different hydrocarbons from the pumping system. The growth of the grain (or its part, Fig. 6) could be thus caused by the synthesis of a layer of some material at the affected part of the grain surface. If this interpretation of the grain growth in Fig. 6 is correct, a role of energetic electrons in this synthesis is crucial because the growth is limited to the part of the grain surface that is affected by the electron beam.

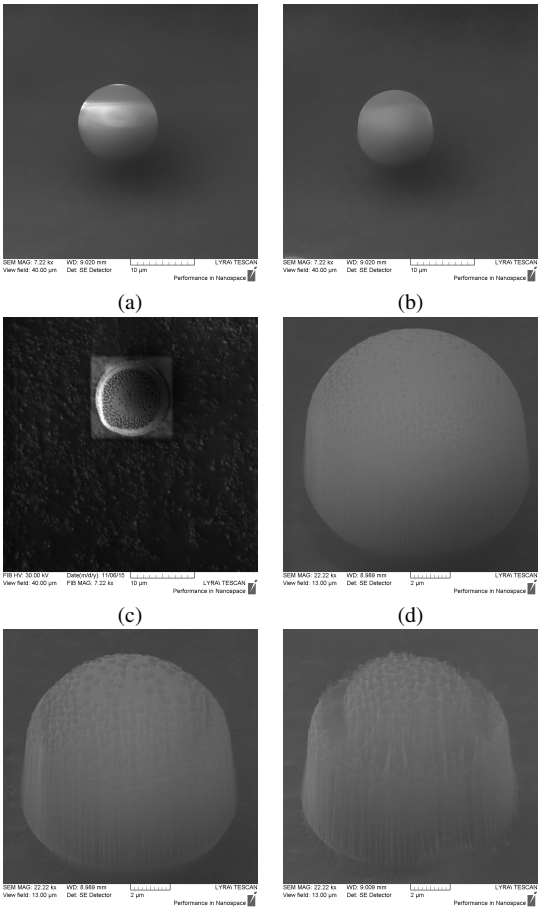

Fig. 10. Sputtering of a spherical MF grain by 30-keV Ga ions (beam intensity: 1.0 A/m^2): (a) prior to sputtering; (b) after 60 s of sputtering; (c) after 150 s — the view from top by FIB; (d) a detail of (c) by the SEM image; (e) after 300 s of sputtering; and (f) another grain sputtered for 540 s.

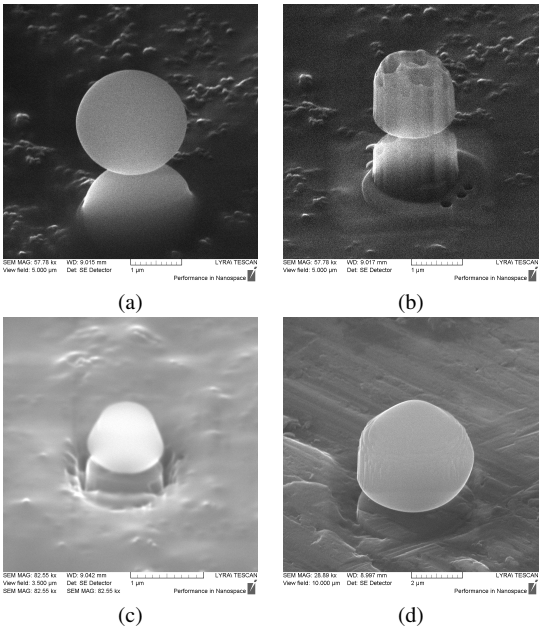

Fig. 11. Sputtering of spherical grains by 30-keV Ga ions: (a) the MF grain prior to; and (b) after 10 s of sputtering (ion beam intensity: 24.3 A/m^2); (c) the SiO_2 grain (ion beam intensity: 0.9 A/m^2, sputtering time: 90 s); and (d) the glassy carbon grain (8.8 A/m^2, 180 s).

We assume that the observed peeling off metallic surface layers that cover the MF grains is connected with the changes of dimensions of the grain inside the layer due to evaporation of volatile components in vacuum that can be amplified by energetic electrons that penetrated through the surface layer. This penetration is rather probable because the surface layers were found to be much thinner than the manufacturer declares.

We have determined the MF work function (4.5 eV) and its value was not affected by the bombardment with low-energy electrons (0.4 keV). The changes of the work function observed in experiments of Pavlu et al. [24] were most probably caused by the aforementioned effects of the large electric field at the grain surface and bombardment by energetic electrons.

We did not determine the sputtering yield but a comparison of photos of the MF grain and the grains from other materials shows that it would be comparable with the sputtering yield measured on SiO_2 spheres of similar diameter [27] but an overall shape of partially sputtered MF grains suggests that the angular dependence of the MF resin sputtering yield would be stronger. Sputtering is not homogenous; it forms grains to a cylindrical shape with milled holes throughout the entire volume. Such effect is observed even for large grains. Although it is hard to estimate the effect of the low-energy ion bombardment (e.g., in the discharge plasma), some peculiarities can be expected.

V. Conclusion

Our study and many already published reports have shown that the MF microspheres cannot to be recommended for applications where a stability of grain parameters is essential. SiO_2 grains that exhibit similar properties could be considered as a more suitable solution for dusty plasma experiments.

Acknowledgment

The authors appreciate help of J. Novakova and I. Khalakhan with SEM imaging and would like to to express their thanks to Prof. D. Vítek for fruitful discussions.

References

[1] G. Morfill, H. Thomas, B. Annaratone, A. Ivlev, R. Quinn, A. Nefedov, V. Fortov, and P.-N. Team, "Complex plasmas under microgravity conditions: First results from PKE-Nefedov," in *Dusty Plasmas in the New Millennium*, ser. AIP Conference Proceedings, R. Bharuthram, M. A. Hellberg, P. K. Shukla, and F. Verheest, Eds., vol. 649. Melville, New York: American Institute of Physics, 2002, pp. 91–109.

[2] A. Nefedov, G. Morfill, V. Fortov, H. Thomas, H. Rothermel, T. Hagl, A. Ivlev, M. Zuzic, B. Klumov, A. Lipaev, V. Molotkov, O. Petrov, Y. Gidzenko, S. Krikalev, W. Shepherd, A. Ivanov, M. Roth, H. Binnenbruck, J. Goree, and Y. Semenov, "PKE-Nefedov: plasma crystal experiments on the International Space Station," *New J. Phys.*, vol. 5, Apr. 2003.

[3] R. Seurig, G. Morfill, V. Fortov, and P. Hofmann, "Complex plasma research on ISS PKE-Nefedov, PK-3 Plus, PK-4, and impact laboratory," *Acta Astronaut.*, vol. 65, no. 5-6, pp. 651–656, 2009.

[4] H. Kersten, H. Deutsch, M. Otte, G. Swinkels, and G. Kroesen, "Microdisperse particles as probes for plasma surface interaction," *Thin Solid Films*, vol. 377-378, pp. 530–536, 2000.

[5] P. Hartmann, A. Z. Kovács, J. C. Reyes, L. S. Matthews, and T. W. Hyde, "Dust as probe for horizontal field distribution in low pressure gas discharges," *Plasma Sources Sci. T.*, vol. 23, no. 4, p. 045008, 2014. [Online]. Available: http://stacks.iop.org/0963-0252/23/i=4/a=045008

[6] M. Dropmann, R. Laufer, G. Herdrich, L. S. Matthews, and T. W. Hyde, "Analysis of magnetic field plasma interactions using microparticles as probes," *Phys. Rev. E*, vol. 92, p. 023107, Aug 2015.

[7] M. Puttscher and A. Melzer, "Dust particles under the influence of crossed electric and magnetic fields in the sheath of an rf discharge," *Phys. Plasmas*, vol. 21, no. 12, p. 123704, 2014.

[8] V. Land, A. Douglass, K. Qiao, L. Matthews, and T. Hyde, "The effect of dust charge variation, due to ion flow and electron depletion, on dust levitation," in *Dusty/Complex Plasmas: Basic and Interdisciplinary Research*, ser. AIP Conference Proceedings, V. Y. Nosenko, P. K. Shukla, M. H. Thoma, and H. M. Thomas, Eds., vol. 1397, no. 1. Melville, New York: American Institute of Physics, 2011, pp. 98–103.

[9] V. Land, A. Douglass, K. Qiao, Z. Zhang, L. S. Matthews, and T. Hyde, "Glow and dust in plasma boundaries," *IEEE Trans. Plasma Sci.*, vol. 41, no. 4, pp. 799–803, April 2013.

[10] A. Douglass, V. Land, K. Qiao, L. Matthews, and T. Hyde, "Determination of the levitation limits of dust particles within the sheath in complex plasma experiments," *Phys. Plasmas*, vol. 19, no. 1, p. 013707, 2012.

[11] M. Schwabe, S. Zhdanov, C. Räth, D. B. Graves, H. M. Thomas, and G. E. Morfill, "Collective effects in vortex movements in complex plasmas," *Phys. Rev. Lett.*, vol. 112, p. 115002, Mar 2014.

[12] B. Liu, J. Goree, V. Nosenko, and L. Boufendi, "Radiation pressure and gas drag forces on a melamine-formaldehyde microsphere in a dusty plasma," *Phys. Plasmas*, vol. 10, no. 1, pp. 9–20, 2003.

[13] X. Wang, M. Horányi, and S. Robertson, "Experiments on dust transport in plasma to investigate the origin of the lunar horizon glow," *J. Geophys. Res.*, vol. 114, no. A5, p. A05103, 2009.

[14] J. Pavlů, A. Velyhan, I. Richterová, Z. Němeček, J. Šafránková, I. Čermák, and P. Žilavý, "Mass-loss rate for MF resin microspheres," *IEEE Trans. Plasma Sci.*, vol. 32, no. 2, pp. 704–708, 2004.

[15] J. Carstensen, H. Jung, F. Greiner, and A. Piel, "Mass changes of microparticles in a plasma observed by a phase-resolved resonance method," *Phys. Plasmas*, vol. 18, no. 3, 2011.

[16] C. Killer, M. Mulsow, and A. Melzer, "Spatio-temporal evolution of the dust particle size distribution in dusty argon rf plasmas," *Plasma Sources Sci. T.*, vol. 24, no. 2, p. 025029, 2015.

[17] W. Paul and H. Steinwedel, "Apparatus for separating charged particles of different specific charges," German Patent, Patent 944,900, 1956.

[18] M. Beranek, I. Cermak, Z. Nemecek, J. Safrankova, M. Jerab, and J. Pavlu, "Linear trap with three orthogonal quadrupole fields for dust charging experiments," *Rev. Sci. Instrum.*, vol. 83, no. 11, p. 115109, 2012.

[19] J. Pavlů, I. Richterová, Z. Němeček, J. Šafránková, and I. Čermák, "Interaction between single dust grains and ions or electrons: laboratory measurements and their consequences for the dust dynamics," *Faraday Discuss.*, vol. 137, pp. 139–155, 2008.

[20] L. Nouzák, I. Richterová, J. Pavlů, Z. Němeček, and J. Šafránková, "Investigations of photoemission from lunar dust simulant," *IEEE Trans. Plasma Sci.*, vol. 44, no. 4, pp. 512–518, 2016.

[21] G. Swinkels, E. Stoffels, W. Stoffels, N. Simons, G. Kroesen, and F. de Hoog, "Treatment of dust particles in an RF plasma monitored by Mie scattering rotating compensator ellipsometry," *Pure Appl. Chem.*, vol. 70, no. 6, pp. 1151–1156, Jun. 1998.

[22] W. W. Stoffels, E. Stoffels, G. H. P. M. Swinkels, M. Boufnichel, and G. M. W. Kroesen, "Etching a single micrometer-size particle in a plasma," *Phys. Rev. E*, vol. 59, pp. 2302–2304, Feb 1999.

[23] I. Richterová, J. Pavlů, Z. Němeček, J. Šafránková, and M. Jeřáb, "Electric field influence on secondary emission," in *New Vistas in Physics of Dusty Plasmas*, ser. AIP Conference Proceedings, L. Boufendi, M. Mikikian, and P. K. Shukla, Eds., vol. 799. Melville, New York: American Institute of Physics, 2005, pp. 395–398.

[24] J. Pavlů, I. Richterová, D. Fujita, J. Šafránková, and Z. Němeček, "Changes of dust grain properties under particle bombardment," in *Multifacets of Dusty Plasmas*, ser. AIP Conference Proceedings, J. T. Mendonça, D. P. Resendesm, and P. K. Shukla, Eds., vol. 1041. Melville, New York: American Institute of Physics, 2008, pp. 299–300.

[25] I. Richterová, J. Pavlů, Z. Němeček, J. Šafránková, and P. Žilavý, "Secondary emission from dust grains with a surface layer: Comparison between experimental and model results," *Adv. Sp. Res.*, vol. 38, no. 11, pp. 2551–2557, 2006.

[26] H. Fiedler, private communication, Volmerstr. 9A, H.3.51, D-12489 Berlin, Germany, 2002/2003.

[27] M. Vyšinka, Z. Němeček, J. Šafránková, J. Pavlů, J. Vaverka, and J. Lavková, "Sputtering of spherical sio2 samples," *IEEE Trans. Plasma Sci.*, vol. 44, no. 6, pp. 1036–1044, 2016.

[28] G. M. McCracken, "The behaviour of surfaces under ion bombardment," *Rep. Prog. Phys.*, vol. 38, no. 2, p. 241, 1975.

[29] P. F. A. Alkemade, "Propulsion of ripples on glass by ion bombardment," *Phys. Rev. Lett.*, vol. 96, p. 107602, Mar 2006.